Inorganic Chemistry

Article

pubs.acs.org/IC

Photosolvolysis of *cis*-[Ru(α-diimine)$_2$(4-aminopyridine)$_2$]$^{2+}$ Complexes: Photophysical, Spectroscopic, and Density Functional Theory Analysis

Mariana R. Camilo,[†] Carolina R. Cardoso,[†] Rose M. Carlos,*[,†] and A. B. P. Lever*[,‡]

[†]Departamento de Química, Universidade Federal de São Carlos, CP 676, CEP 13565-905, São Carlos-SP, Brazil

[‡]Department of Chemistry, York University, 4700 Keele St., North York, Toronto, Ontario, Canada M3J1P3

Supporting Information

ABSTRACT: The photochemical and photophysical properties of the *cis*-[Ru^{II}(α-diimine)$_2$(4-APy)$_2$]$^{2+}$ complexes, where α-diimine = 1,10-phenanthroline (phen) and 4-APy = 4-aminopyridine **I**, 4,7-diphenyl-1,10-phenanthroline (Ph$_2$phen) **II**, 2,2′-bipyridine (bpy) **III**, and 4,4′-dimethyl-2,2′-bipyridine (Me$_2$bpy) **IV**, are reported. The four complexes were characterized using high-performance liquid chromatography, ^{1}H NMR, UV−visible, emission, and transient absorption spectroscopy. Upon photolysis in acetonitrile solution these complexes undergo 4-APy dissociation to give the monoacetonitrile complex (for **II**, **III**, and **IV**) or the bis(acetonitrile) complex (for **I**). A fairly wide range of excitation wavelengths (from 420 to 580 nm) were employed to explore the photophysics of these systems. Quantum yields and transient spectra are provided. Density functional theory (DFT) and time-dependent DFT analysis of singlet and triplet excited states facilitated our understanding of the photochemical behavior. A detailed assessment of the geometric and electronic structures of the lowest energy spin triplet charge transfer state (^{3}MLCT) and spin triplet metal centered state (^{3}MC) (d$\pi \rightarrow \sigma^*$ transitions) for species **I**−**IV** is presented. A second, previously unobserved, and nondissociative, ^{3}MC state is identified and is likely involved in the primary step of photodissociation. This new ^{3}MC state may indeed play a major role in many other photodissociation processes.

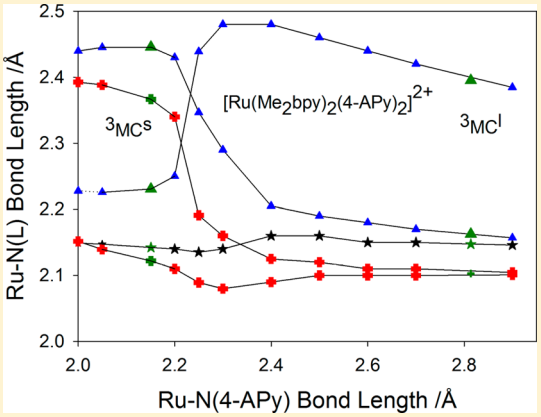

INTRODUCTION

The investigation of spectroscopic, electrochemical, photochemical, and photophysical properties of Ru^{II} complexes of the type *cis*-[Ru(α-diimine)$_2$L$_2$]$^{2+}$ (L = electron donor/acceptor ligand) has attracted much attention because of the potential application of these compounds in diverse areas of science, particularly as emissive probes and photochemical delivery agents.[1−13]

Many examples of photosubstitution reactions in luminescent complexes have been reported for ruthenium complexes of (mostly) 2,2′-bipyridine combined with various photolabile ligands (L), for example L = acetonitrile, 3,6-dithiaoctane and other sulfur ligands, serotonin, ethylenediamine, tryptamine, 3-aminopyridine, 4-aminopyridine, γ-aminobutyric acid (GABA), butylamine, and tyramine, etc.[3,8,14−27]

It is now generally understood that the mechanism of photosubstitution involves excitation to a singlet metal-to-ligand charge transfer state (^{1}MLCT) followed by intersystem crossing to the lowest spin triplet charge transfer state (^{3}MLCT). This is then deactivated by crossing to a spin triplet metal centered state (^{3}MC), leading to photosubstitution.[19,27−53]

Bis(bipyridine) ruthenium complexes with 4-aminopyridine have been fairly extensively investigated photochemically[16,41,54−56] and by density functional theory (DFT),[19,22] as have similar complexes with the unsubstituted pyridine.[17,31,44] Of particular note is a minimum in the lowest excited state potential energy surface when one 4-aminopyridine is moved about 2.8 Å away from ruthenium.[16] This is associated with a conical intersection between this ^{3}MLCT state and a metal centered $\pi-\sigma^*$ ^{3}MC state.[57]

A very recent study[44] explores this in detail for the unsubstituted pyridine analog. In particular Lamberti et al.[44] propose, using DFT and X-ray transient absorption spectroscopy, that in *cis*-[Ru(bpy)$_2$(Py)$_2$]$^{2+}$ there is a ^{3}MC lying about 0.4 eV (depending on choice of functional and basis set) below the lowest ^{3}MLCT. Photosolvolysis then proceeds via population of this ^{3}MC state.

The present work employs L = 4-aminopyridine (4-APy) and extends the previous work by

(i) presenting data for other diimines, specifically 1,10-phenanthroline (phen), 4,7-diphenyl-1,10-phenanthro-

Received: January 3, 2014
Published: March 12, 2014

   dx.doi.org/10.1021/ic5000205 | *Inorg. Chem.* 2014, 53, 3694−3708

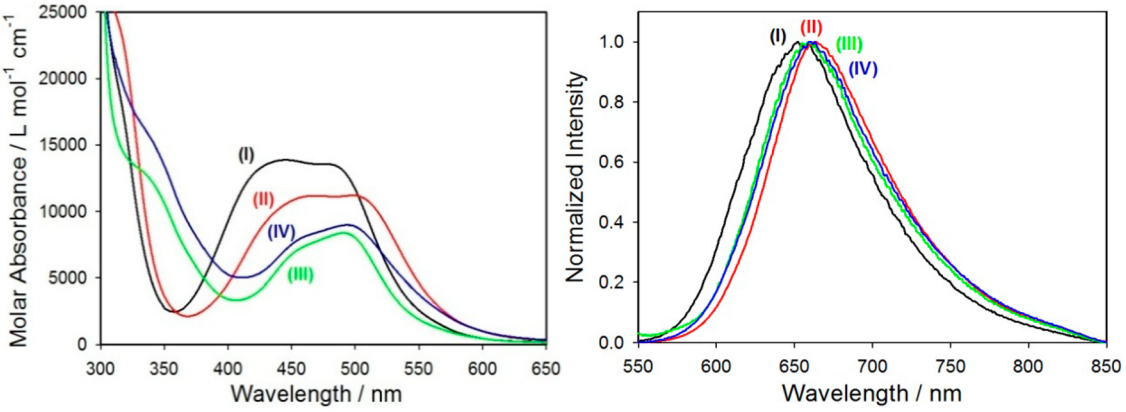

Figure 1. Visible region spectra (normalized) (λ_{exc} = 450 nm) of species **I** to **IV** as identified in acetonitrile. (left) Absorption. (right) Emission.

line (Ph_2phen), 4,4′-dimethyl-2,2′-bipyridine (Me_2bpy), as well as providing additional data for 2,2′-bipyridine.

(ii) demonstrating that photosolvolysis to form *cis*-[Ru(α-diimine)$_2$L(CH_3CN)]$^{2+}$ can occur with very low energy light, specifically at 580 nm, and that the quantum yield of the low energy process is essentially identical to that at higher energy (480 nm). For diimine = phen, the monoacetonitrile species is also photoactive, leading to loss of both 4APy ligands.

(iii) postulating a change in conformation between ground state and lowest ^{3}MLCT state.

(iv) providing electronic absorption spectra of the ground state and transient absorption spectra of the ^{3}MLCT state for these species, both fitted by time-dependent (TD) DFT calculations. Emission and excitation spectra, of the parent species, are also reported.

(v) exploring the potential energy, excited state, surfaces of these low lying states as a function of Ru−N(4-APy) bond length coordinate, thereby providing geometric and electronic structural data for the DFT geometry-optimized ^{3}MLCT and ^{3}MC states of these species, and evaluating their relative energies.

(vi) identifying a hitherto undetected, nondissociative, ^{3}MC state that most likely plays a major role in the photosolvolysis pathway.

(vii) exploring the extent of configurational interaction between the ^{3}MLCT and the two ^{3}MC states.

RESULTS AND DISCUSSION

Synthesis and Characterization of Complexes I−IV. The luminescent complexes **I**−**IV** were synthesized by the reaction of 4-aminopyridine with[58] *cis*-[Ru(α-diimine)$_2$(OH_2)$_2$]$^{2+}$ (**I, III**, and **IV**) and *cis*-[Ru(α-diimine)Cl_2]$^{2+}$ (**II**) in an ethanol/H_2O mixture using a procedure similar to one already established.[2−7,16,55,59,60] The complexes were characterized by elemental analysis, cyclic voltammetry, analytical high-performance liquid chromatography (HPLC), and ^{1}H NMR. X-ray data are also available.[55,61]

^{1}H NMR. CD_3CN solutions of (**I**−**IV**) were characterized using NMR spectroscopy (Supporting Information, Table S1, Figures S1 and S2). Supporting Information, Figure S2 shows the proton chemical shifts of the four complexes. Since the methyl group is weakly electron-donating, the H5 and H6 signals in complex **IV** show upfield shifted resonances compared with those of complex **III**. Substituting the bpy ligand for phen causes a shift in the H6 signal from 8.92 to 9.35. Substituting phenyl groups causes an even larger H6 downfield shift, in accordance with the stronger electron withdrawing effect of the phenyl substituent.

The two α-protons on the APy ligands are equivalent and could not be distinguished using lower temperature (to 0 °C) NMR. As noted below there are two conformations of the APy ligands, and these NMR data require either that there is predominantly one conformer in solution, or that interconversion between them is faster than the NMR time scale. Detailed NMR data are provided in Supporting Information.

Molecular Structure. The crystal structure of complex **III** has been described previously.[55] We describe elsewhere[61] the first reported X-ray structure of complex **I** and a second structure of **III** with a different counterion from the previous analysis.[61] Each complex shows the Ru atom bound to two α-diimine ligands in a cis configuration with the two 4-APy ligands. The Ru−N(α-diimine) distances, ∼2.070 Å, are similar to those in [Ru(bpy)$_3$)]$^{2+}$ (2.056 Å).[62,63]

Each 4-aminopyridine ligand is perpendicular to one α-diimine and is canted ca. 65−70° out of the plane of the other 4-aminopyridine. There are two important possible conformations of these complexes, with the planes of the 4-aminopyridine ligands oriented over a void in the structure (the "void" conformer) or over the center of the opposing α-diimine ligand (the "over center" conformer). We discuss this further below.

UV−Visible Spectroscopy. The absorption spectra of the four complexes in acetonitrile solution show strong UV absorption mostly $\pi-\pi^*$ in origin and broad structured absorption in the visible (vis) region around 450−500 nm (Figure 1 (left) and Supporting Information, Figure S3, Table 1), indicative of overlapping transitions to different MLCT states.[16,31,41,64,65]

Emission Spectra. When excited, for example, at 450 nm, complexes **I**−**IV** produce an intense and broad emission band with a maximum at about 660 nm (uncorrected) (Figure 1 (right) and Table 1) with energies and lifetimes typical for species of this type.[49,65] For all four complexes the emission decay profiles measured in CH_3CN (Table 2, Supporting Information, Figure S3A) and dimethylformamide (DMF) (Supporting Information, Table S2, Figure S3B) solution required biexponential fits, suggesting the presence of two emitting processes, one of which heavily dominates. As mentioned above, there are two conformers of these species depending on the relative orientation of the 4-APy ligands. The two emitting species seem to have essentially identical UV−vis

dx.doi.org/10.1021/ic5000205 | Inorg. Chem. 2014, 53, 3694−3708

Table 1. Experimental UV−Visible Absorption and Emission Maxima for Complexes I−IV in Acetonitrile at Room Temperature

complex	electronic absorption $\nu/10^3$ cm^{-1} (log ε)	emission $\nu/10^3$ cm^{-1} (λ_{exc} = 450 nm)
I	20.7 (4.13), 22.8 (4.14), 37.5 (4.97), 44.6 (4.85)	15.3
II	20.0 (4.05), 22.0 (4.04), 31.5 sh (4.38), 36.0 (4.84), 42.2 (4.53), 44.8 (4.65)	15.1
III	20.0 (3.89), 22.2 sh (3.85), 29.2 (4.06), 34.0 (4.68), 40.6 (4.42)	15.3
IV	20.4 (3.95), 22.3 sh (3.87), 34.5 (4.73), 41.1 (4.53)	15.1
CH_3CN complex		
I·$(CH_3CN)_2$	23.5 (4.12), 34.0 sh (4.45), 37.9 (5.02), 44.4 (4.92)	
II·(CH_3CN)	22.7 (4.09), 31.8 sh (4.34), 36.1 (4.86), 42.1 sh (4.61)	
III·(CH_3CN)	22.2 (3.88), 29.8 sh (3.97), 34.9 (4.78), 41.5 (4.59)	
IV·(CH_3CN)	22.3 (3.91), 34.9 (4.79), 39.06 sh (4.46), 41.3 (4.61)	

spectra, and so it is likely that they arise from these two conformers, one of which is dominant (see below).

The emission of species **III** has been reported previously[55] as a single exponential decay with a lifetime of ca. 460 ns, also in acetonitrile; the reason for such a large discrepancy with our work is unknown. The related species $[Ru(Me_2\text{-}bpy)_2(Py)_2]^{2+}$ emits at 15 000 cm^{-1} in EtOH/MeOH (4:1), with a room-temperature lifetime of 20 ns.[35] The species $[Ru(bpy)_2(Py)_2]^{2+}$ does not emit at room temperature for reasons noted below, but at 77 K it does emit at 17 000 cm^{-1}.[66]

Excitation Spectra. The excitation spectrum of complex **III** at λ_{em} = 640 nm, shown in Figure 2 and Supporting Information, Figure S4, is independent of the monitoring wavelength within the emission band range of 630−690 nm. The excitation spectrum reaches a maximum close to the same wavelength as the visible region absorption. These data are fully consistent with previous literature data on the same or similar compounds.[31,54,55]

Transient Absorption Spectra. The transient absorption spectra of complexes **I**−**IV** in acetonitrile are similar to that of the $[Ru(bpy)_3]^{2+}$ complex and related complexes.[8,67−72] For example, Figure 3 shows the excited state absorption spectrum for complex **II** in CH_3CN solution after excitation with an 8 ns pulse at 355 nm (λ_{exc}). There is bleaching of the absorption band at 480 nm and new absorption with maxima at 350 nm and around 590 nm. The transient absorption spectra of complexes **II**−**IV**, which are similar, are given in Supporting Information (Figure S5). We note that, in principle, the photosubstitution process could be very fast and occur during the lifetime of the pulse, in which case the transient spectrum would correspond with the spectrum of the ground state of the photoproduct. Since the mono-CH_3CN species has strong absorption around 500 nm, it is obviously (see Figure 3) not

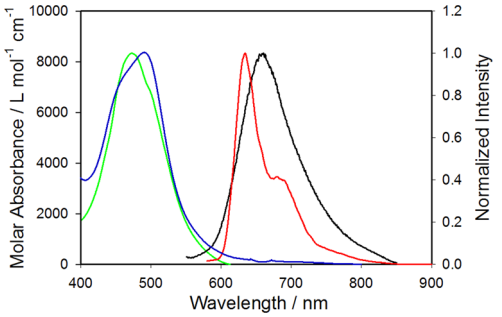

Figure 2. Excitation spectrum (green), UV−vis absorption spectrum (blue), and (uncorrected) emission spectrum (λ_{exc} = 450 nm) at room temperature in acetonitrile (black), and (uncorrected) emission spectrum at 77 K in MeOH/EtOH (4:1) (red) of complex **III** (1.0 × 10^{-6} mol L^{-1}). Molar absorbance scale applies only to the absorption spectrum.

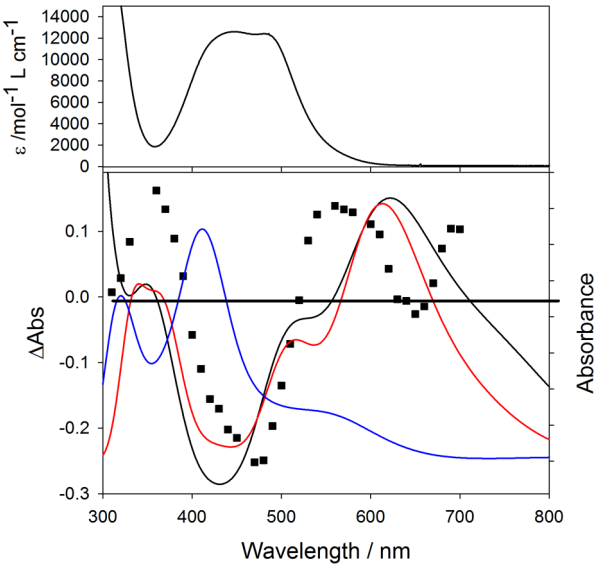

Figure 3. Experimental absorption spectrum (upper) and transient spectrum (lower, dotted, left *y* axis) of complex **I** in acetonitrile solution (λ_{exc} = 355 nm and 8 ns pulse; spectrum recorded at *t* = 10 ns following excitation). The TD-DFT predicted spectra of the optimized, lowest energy, ^{3}MLCT and ^{3}MC states are also shown (^{3}MLCT, red, center conformation, green, void conformation; ^{3}MC, blue).

Table 2. Excited-State Lifetimes (τ_i), Pre-Exponential Factor (b_i) Obtained from Biexponential Fit Decay Profiles[a] for Complexes I−IV in Acetonitrile at Room Temperature

complex	τ_1 (ns)	τ_2 (ns)	b_1	b_2	χ^2_{red}	%$_1$	%$_2$
I−phen	75	16	8500	1200	1.07	97.0	3.0
II−Ph_2phen	665	91	7300	1000	1.18	98.1	1.9
III−bpy	73	13	8100	1500	1.18	96.8	3.2
IV−Me_2bpy	102	15	7800	1100	1.13	97.9	2.1

[a] $I(t) = \sum_i b_i e^{-t/\tau_i}$; excitation and emission wavelengths were 460 and 660 nm, respectively, and the complex concentration was 2.0 × 10^{-5} mol L^{-1}. The quality of the fit was judged by the analysis of the statistical parameter reduced χ^2 value and by inspection of the residuals distribution. The percentage values in Table 2 give the contribution to the total phosphorescence emission.

dx.doi.org/10.1021/ic5000205 | Inorg. Chem. 2014, 53, 3694−3708

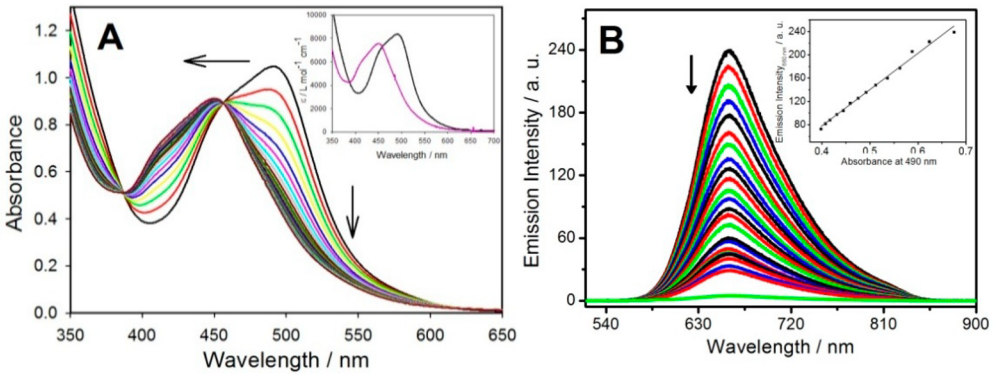

Figure 4. Photosolvolysis of complex **III** (1.02×10^{-4} mol L^{-1}) with 480 nm light ($I_0 = 9.52 \times 10^{-9}$ einstein s^{-1}) in acetonitrile; total irradiation time = 104 min. (a) Change in the absorption spectrum; inset, plot of visible region spectra of species **III** (black) and **III**·CH_3CN (purple). (b) Response of the emission spectra during the progress of photolysis; inset, plot of emission intensity versus absorbance at 490 nm.

being formed in significant quantity during the lifetime of the pulse. However, in general such photoprocesses may occur extremely rapidly.[73,74] Interestingly, a recent study does reveal that a similar photosubstitution process, in *cis*-$[Ru(bpy)_2(py)_2]Cl_2$, occurs within a much longer pulse of 800 ns.[17] Note that the negative pit around 650 nm is due to emission of the ground state species in this region such that the apparent peak growing near 700 nm is not real but is likely a tail from the 600 nm peak. The TD-DFT predicted optical spectra of the equilibrated ^{3}MLCT state, in the center and void conformations, and ^{3}MC state are also shown in Figure 3 and discussed below.

Electrochemistry. The cyclic voltammograms of the four Ru^{II} complexes, at a platinum electrode, exhibit a well-defined metal-based redox ($Ru^{III/II}$ couple in the range of 1−1.3 V versus AgCl/Ag (100 mV s^{-1}), as observed extensively in the past[31,65,75,76] (Supporting Information, Figure S6). Two reduction processes are also generally seen (Supporting Information, Figure S7); they can be assigned to sequential addition of an electron to the π^*−LUMO (LUMO = lowest unoccupied molecular orbital) of each bound α-diimine ligand.[65] This is well-known behavior and is not further discussed.

Photochemistry. When solutions of complexes **II**, **III**, and **IV** were subject to continuous photolysis the resulting optical spectroscopic changes (UV−vis, luminescence, and ^{1}H NMR (Figure 4 and Supporting Information, Figures S8−S10)) were consistent with the substitution of one 4-APy ligand by a solvent molecule (eq 1), in agreement with earlier studies with 4-aminopyridine and related systems.[15−17,19,22,40,77]

$$cis\text{-}[Ru(\alpha\text{-diimine})_2(4\text{-APy})_2]^{2+} + CH_3CN \rightarrow cis\text{-}[Ru(\alpha\text{-diimine})_2(4\text{-APy})(CH_3CN)]^{2+} + 4\text{-APy} \quad (1)$$

For example, Figure 4a illustrates the spectroscopic changes seen when an acetonitrile solution of complex **III** was irradiated at 480 nm. The spectra show a progressive depletion of the absorption band at 490 nm concomitant with growth of absorption at ca. 440 nm (Figure 4a). Exhaustive photolysis (2 h) leads to a final stable spectrum. No back-reaction is observed when the light is turned off. When photolysis was monitored by luminescence spectroscopy, the emission band at 660 nm disappeared, and no new band appeared in this region (Figure 4b), indicating that the mono-CH_3CN species is nonemissive. The UV−vis spectroscopic changes of this solution recorded parallel with those described above, and plots of optical spectra band intensity changes versus changes in the maximum emission band, were linear, implying a one-to-one correspondence (Figure 4b, inset). Continuous photolysis experiments carried out for compounds **II** and **IV** led to similar spectroscopic results, Supporting Information, Figures S8 and S10, consistent with earlier studies.[16,18−20,22,31,36] The resulting monoacetonitrile complexes were identified by NMR.

The photolysis of complex **I** in CH_3CN differs from the other complexes studied in this work. A progressive depletion of the absorption band is noted at 450−490 nm (Supporting Information, Figure S11) with concomitant blue shifts to 440 nm (eq 1) and then a subsequent blue shift to 420 nm as the process in eq 2 becomes dominant. The absorption spectrum of the solution at the end of the photolysis corresponds with that of *cis*-$[Ru(phen)_2(CH_3CN)_2]^{2+}$. Electrochemically, during the course of the photolysis, one can observe the successive formation of the mono- and bis-acetonitrile species by their cyclovoltammetric signatures (Figure 5). The shift to more positive potentials for the $Ru^{III/III}$ process, on successive substitution, is entirely in line with expectation based on ligand electrochemical parameters,[76] that is, a shift of ca. +0.1 V per substitution.

Thus the continued irradiation is associated with successive dissociative processes operating during photolysis:

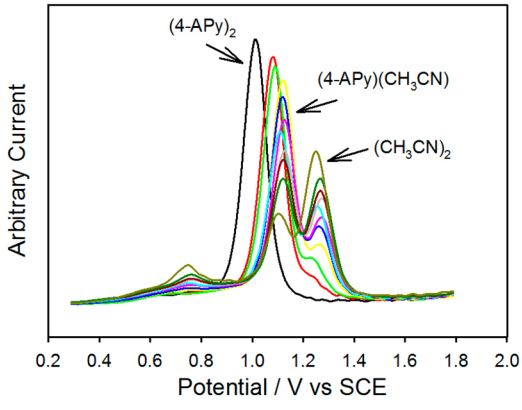

Figure 5. Differential pulse voltammograms of the Ru^{III}/Ru^{II} redox process in steps recorded during the photolysis of species **I**. Successive conversion is observed of *cis*-$[Ru(phen)_2(4\text{-APy})_2]^{2+}$ ($E_{1/2}$ = 1.00 V) to *cis*-$[Ru(phen)_2(4\text{-APy})(CH_3CN)]^{2+}$ ($E_{1/2}$ = 1.11 V) to *cis*-$[Ru(phen)_2(CH_3CN)_2]^{2+}$ ($E_{1/2}$ = 1.25 V)(V vs SCE).

dx.doi.org/10.1021/ic5000205 | Inorg. Chem. 2014, 53, 3694−3708

$$cis\text{-}[Ru(phen)_2(4\text{-}APy)(CH_3CN)]^{2+} + CH_3CN \rightarrow cis\text{-}[Ru(phen)_2(CH_3CN)_2]^{2+} + 4\text{-}APy \quad (2)$$

The loss of the second 4-APy must arise from photoexcitation of the mono-CH_3CN product as it is most improbable that photoexcitation of the parent would cause the loss of both 4-APy ligands. Similar consecutive dual photolyses have been observed previously, for example,[40] 580 nm light is also effective in the photolysis of all four diimine species (**I**–**IV**).

The quantum yields of photolysis, in acetonitrile (Table 3) are essentially independent of the monitoring wavelength within the emission envelope. Given the errors inherent in chemical actinometry, we regard the quantum yields as being essentially independent of excitation wavelength; most significantly, the yield at 580 nm is then essentially identical to that at 480 nm. The yields are typical for such photosubstitution processes.[15,25,27,36−38,78,79] This lack of dependence on excitation energy implies that the photolytically active state is the lowest excited state. Note, for example, increasing quantum yields with shorter wavelength in similar systems where the $\pi-\sigma^*$ state is likely accessible at higher energy.[25,36]

Table 3. Average Quantum Yields of Photolysis of Species II, III, and IV in Acetonitrile as a Function of Exciting Wavelength

excitation, nm	**II**–Ph_2phen[a]	**III**–bpy[a]	**IV**–Me_2bpy[a]
420	0.03	0.05	0.05
480	0.04	0.04	0.07
520	0.04	0.07	0.07
580	0.04	0.09	0.06

[a]These values represent the average of two independent runs. Values for species **I** are not provided because of the two overlapping processes.

Theoretical (DFT) Analysis. A general view of the structures of the four complexes, *cis*-[Ru(α-diimine)$_2$(4-APy)$_2$]$^{2+}$, is shown in Supporting Information, Figure S12. The geometries were DFT-optimized using B3LYP/LANL2DZ inclusive of solvent using the PCM model with acetonitrile.[80,81] This combination reproduces the X-ray crystal structural data of ruthenium α-diimine complexes quite closely, albeit sometimes with somewhat lengthened bond distances (Table 4).[50,53,63,80−90] Selected bond lengths for the optimized geometry in CH_3CN are given in Supporting Information, Table S3, and *xyz* coordinates of the singlet ground state are given in Supporting Information, Tables S13, S16, S19, and S22.

Orientation of the 4-APy planes. There are two important conformations of the 4-APy ligand plane, as shown in Figure 6. In one (left) the plane projects over a void in the geometry of the ligands, while in the other (right), it projects over the center of the opposite chelate ring. The X-ray structures of the phenanthroline **I** and bipyridine **III** complexes reveal that they exist in the void conformation, but this may occur for packing rather than electronic reasons. Of course, one conformation is thermodynamically favored, but it transpires that the second sits in a local minimum of the molecular potential surface. If one starts a geometry optimization of the molecule using either of these conformations, then the program optimizes to a minimum with the same conformation for all

Table 4. Bond Lengths Ru–N(4-APy) in Ground State, Spin Singlet, and Lowest Energy, Excited Spin Triplet ^{3}MLCT States (Equilibrium Geometry) Of the Parent Species I, II, III, and IV and Their Mono-CH_3CN Photolysis Products.[a]

	[Ru(diimine)$_2$(4-APy)$_2$]$^{2+}$				[Ru(diimine)$_2$(4-APy)(CH$_3$CN)]$^{2+}$		
complex	DFT ^{1}g.s. Ru–N (4-APy)	X-ray ^{1}g.s. Ru–N	DFT ^{3}MLCT Ru–N (4-APy$_s$)[b]	DFT ^{3}MLCT Ru–N (4-APy$_l$)[b]	DFT ^{1}g.s. Ru–N(4-APy)	DFT ^{3}MLCT Ru–N(4-APy)	
I–phen	2.15	2.10,[c] 2.12	2.10	2.13_s	2.14	2.10	
II–Ph_2phen	2.15		2.12	2.14	2.14	2.09	
III–bpy	2.15	2.10, 2.12[d]	2.11	2.15	2.15	2.08	
IV–Me_2bpy	2.15		2.11	2.15	2.15	2.09	

[a]Data rounded to two decimal places; more complete data to three decimal places are provided in Supporting Information, Table S3; g.s. = ground state. [b](4-APy$_s$) and (4-APy$_l$) are the short and long bonded 4-aminopyridine ligands, respectively. [c]Reference 61. [d]Reference 55.

dx.doi.org/10.1021/ic5000205 | Inorg. Chem. 2014, 53, 3694−3708

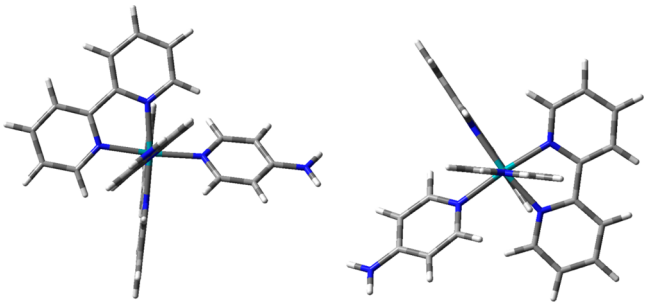

Figure 6. Orientations of the 4-APy ligand planes. (left) Ligand plane over voids in the molecule, and (right) ligand plane over the center of a diimine ligand. One diimine ligand is viewed edge-on.

cases except the ^{3}MLCT state of **III**-void, where rotation to the thermodynamically more stable center conformation occurs. There are certainly precedents for excited states rearranging during photosubstitution events.[74b,91]

The difference in energy between the two configurations is very small and is arguably within the error limits of the DFT process. However, it is interesting that the void conformation is slightly more stable than the over center conformation for all the ground state species, while for the geometry-optimized lowest energy ^{3}MLCT, the reverse is true (Table 5). A similar

Table 5. SCF Energies of the Two 4-APy Conformations in the Ground and Lowest ^{3}MLCT States of $[Ru(diimine)_2(4\text{-}APy)_2]^{2+}$ and $[Ru(diimine)_2(4\text{-}APy)(CH_3CN)]^{2+}$

	void	over center
$Ru(diimine)_2(4\text{-}APy)_2]^{2+1}$ g.s.[a]		
I	(−1844.055 610 95)	−1844.052 19
II	(−2768.133 652 35)[a]	(−2768.133 653 03)[a]
III	(−1691.615 241 82)	−1691.610 841 21
IV	(−1848.872 894 08)	−1848.868 584 72
^{3}MLCT[a]		
I	−1843.980 254 88	(−1843.983 188 26)
II	−2768.063 386 03	(−2768.063 563 28)
III	−1691.543 330 71	(−1691.545 172 90)
IV	−1848.801 753 24	(−1848.803 241)
$[Ru(diimine)_2(4\text{-}APy)(CH_3CN)]^{2+1}$ g.s.[a]		
I	(−1673.176 794 34)	−1673.175 976 49
II	(−2597.255 203 21)	−2597.253 949 55
III	(−1520.736 888 71)	−1520.735 849 65
IV	(−1677.994 883 88)	−1677.993 873 48
^{3}MLCT[a]		
I	−1673.094 086 23	(−1673.097 116 60)
II	−2597.180 830 34	(−2597.181 685 36)
III	*b*	(−1520.664 467 60)
IV	−1677.922 720 71	(−1677.922 725 98)
	void	over center

[a]Optimized energies in Hartrees/mol; lowest energy indicated in (parentheses); g.s. = ground state. [b]Void conformation twists into the over center conformation.

and consistent observation can be made about the ground state and lowest ^{3}MLCT excited states of the mono(acetonitrile) species. Hence, we shall assume void conformations for the ground state and over center conformations for the lowest ^{3}MLCT excited states of these molecules.

Thus there is a conformational change upon excitation to the ^{1}MLCT and relaxation to the ^{3}MLCT. An attempt to prove this involved comparing the experimental transient spectrum with the predicted triplet transient absorption spectra of the ^{3}MLCT state for the two conformations (shown in Figure 3). Not surprisingly, they do not differ a great deal, and both are quite acceptable approximations to the experimental spectrum, so no definitive conclusion can be drawn. Considering the two emitting states observed with these parent species (see above), the proportion of the lesser to the greater component is roughly the same for all four species. We suppose then that these two states arise from the two conformations, with the over center conformation state being the majority emitter.

Singlet Excited States and Absorption Spectra. To demonstrate that the DFT-derived geometries provide an adequate description of the electronic structure of these complexes, the TD-DFT-predicted absorption spectra of complexes **I**−**IV** are compared with the experimental spectra obtained in acetonitrile (Figure 7). The transition energies, oscillator strengths, and assignments are given in Supporting Information, Tables S5−S8. The agreement between the calculated and experimental spectra is acceptably good.

The molecular orbital (MO) composition diagram for the ground state of species **III** (void conformation) is shown in Figure 8 as a guide for the spectroscopic assignments. Similar data for the other complexes are available in Supporting Information (Figure S13, Tables S15, S18, S21, and S24). On the basis of Figure 8 many 4d → π^* diimine MLCT transitions in the visible region are expected, with 4d → π^* 4-aminopyridine transitions closer to the UV region and some higher energy 4-aminopyridine to π^* diimine LL′CT transitions and internal ligand transitions. For all complexes studied, there is broad absorption near 20 000 cm^{-1}, a broad shoulder near 30 000 cm^{-1}, and strong UV absorption centered around 35−40 000 cm^{-1}. Clearly there are many transitions (vertical bars in Figure 7) that contribute to the overall absorption envelope. Nevertheless all the major bands in both the 20 000 and 30 000 cm^{-1} region correspond with MLCT, Ru 4d-to-diimine transitions, with some weaker Ru 4d-to-4-aminopyridine MLCT in the latter region. The strongest UV bands are internal diimine and internal π−π^* 4-APy excitations. L′LCT transitions, 4-APy to diimine, begin around 29 000 cm^{-1}, but they are weak. Detailed assignments are found in Supporting Information, Tables S5−S8. Spin triplet transition energies are also shown in Supporting Information, Tables S9 to S12, and *xyz* coordinates of the ^{3}MLCT state are shown in Supporting Information, Tables S14, S17, S20, and S23. The optical spectra of these types of species are well-understood.[50,64,65,92]

Spin Triplet ^{3}MLCT—Lowest Excited Charge Transfer State. Excitation in the visible region will ultimately lead to intersystem crossing and relaxation to populate the lowest energy ^{3}MLCT state, and information about this state is crucial to an understanding of the photochemistry of these species. We anticipate that this ^{3}MLCT state will be described as a Ru^{III} species containing a reduced polypyridine ligand. The DFT analysis using B3LYP/lanl2dz and the polarizable continuum model (PCM) solvent model with acetonitrile was used to geometry-optimize this lowest spin triplet state. In this ^{3}MLCT state it transpires that the two 4-aminopyridine ligands have markedly different Ru−N(4-APy) bond distances (shown henceforth as $[L,L^-Ru^{III}(4\text{-}APy_s)(4\text{-}APy_l)]^{2+}$) (Table 4), where 4-APy$_s$ and 4-APy$_l$ are the 4-aminopyridine ligands at the shorter and longer distances, respectively, and L^- is the reduced polypyridine ligand. Differing Ru−N distances in the ^{3}MLCT state have been noted previously.[15−17,20,44,48,50,53]

dx.doi.org/10.1021/ic5000205 | *Inorg. Chem.* 2014, 53, 3694−3708

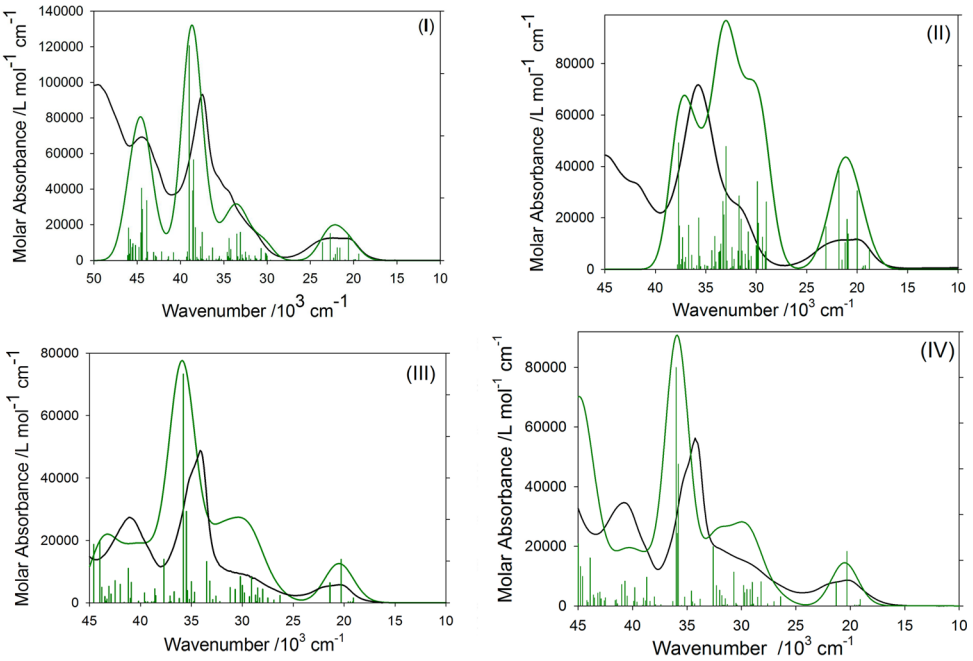

Figure 7. Experimental in CH_3CN (black line) and calculated TD-DFT, PCM (acetonitrile) (dark green line) electronic absorption spectra of complexes **I**–**IV**. The electronic transitions are identified by their relative oscillator strengths (bar graph in dark green).

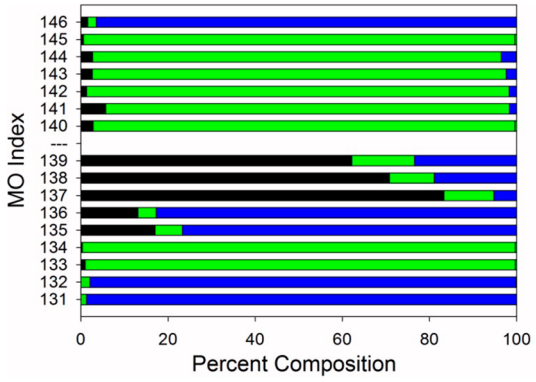

Figure 8. Percentage contributions to the frontier molecular orbitals of the spin singlet ground state of species **III** (void conformation). Ruthenium, black; α-diimine, green; 4-aminopyridine, blue. Highest occupied molecular orbital (HOMO) = #139 B3LYP/Lanl2dz PCM CH_3CN.

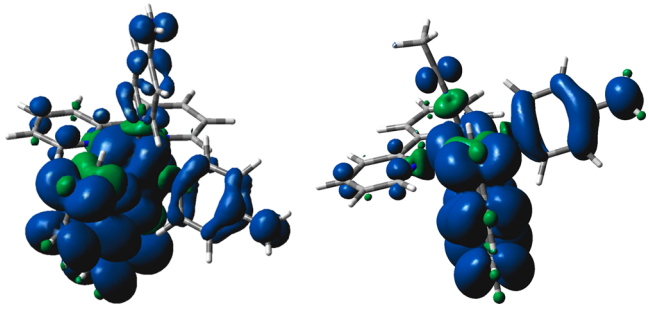

Figure 9. (left) The S = 1 spin density distribution in the geometry-optimized ^{3}MLCT state, $[Ru(diimine)(diiminato)(4\text{-}APy_s)(4\text{-}APy_l)]^{2+}$, (diimine = 2,2′-bipyridine, center conformation). The short bonded ligand 4-APy_s lies to the bottom right of this graphic, and 4-APy_l points up at the top. (right) The S = 1 spin density distribution in the geometry-optimized ^{3}MLCT state, $Ru(diimine)(diiminato)(4\text{-}APy)(CH_3CN)]^{2+}$. The unreduced bipyridine can be seen at the back.

The solvent continuum analysis reveals the ^{3}MLCT excited state indeed to be $[Ru^{III}(diimine)(diiminato(1-))(4\text{-}APy_s)(4\text{-}APy_l)]$ where diiminato(1-) is a localized, one-electron reduced diimine. Spin is distributed ca. 0.9–1.0 on Ru and ca. 1.05 on one negatively charged (ca. −0.2e) diiminato ligand (Supporting Information, Table S4). In all the parent bis-4-APy species, the longer bonded 4-APy_s lies trans to the reduced diiminato(1-) ligand (Figure 9).

Further, in the ^{3}MLCT state of all four parent species, the Ru–N (diiminato) bonds are shorter than the Ru–N(diimine) bonds (Supporting Information, Table S3) presumably because of an extra electrostatic contribution. The two diimine ligands are clearly distinguished by the integral spin on one (diiminato) and zero spin on the other (diimine) (Figure 9) and by the much less positive, indeed negative, charge, on the diiminato ligand relative to the diimine. The ruthenium (Ru^{III}) in the ^{3}MLCT state has a spin density approaching unity. This structure, of course, is reminiscent of the localized $[Ru^{III}(bpy)_2(bpy^-)]^{2+*}$ structure of the ^{3}MLCT excited state of $[Ru^{II}(bpy)_3]^{2+}$ in solution.[93,94] Similar data for the ^{3}MLCT of the unsubstituted pyridine analog are provided by Sadler.[44]

We show in Figure 10 the breakdown of the frontier spin–orbitals of the ^{3}MLCT state into contributions from the various components of the complexes. In the α-manifold, the α-HOMO in all four species is essentially localized on the diiminato ligand, while the α-LUMO and α-LUMO+1 are localized on the diimine ligand. The frontier MOs are fairly well localized on each 4-APy ligand, with little mixing between them. Thus the α-HOMO-1,-2 in **I**, **III**, and **IV** (α-HOMO-2,-3 in **II**) are localized predominantly on the 4-APy_l and 4-APy_s ligands, respectively. Lower lying MOs however reveal greater mixing between the two 4-APy ligands. In species **III**, the α–dσ* MOs are #149,150 lying ca. 2.6–2.7 eV above the ^{3}MLCT α-manifold HOMO. They are similarly placed in the other species.

dx.doi.org/10.1021/ic5000205 | Inorg. Chem. 2014, 53, 3694–3708

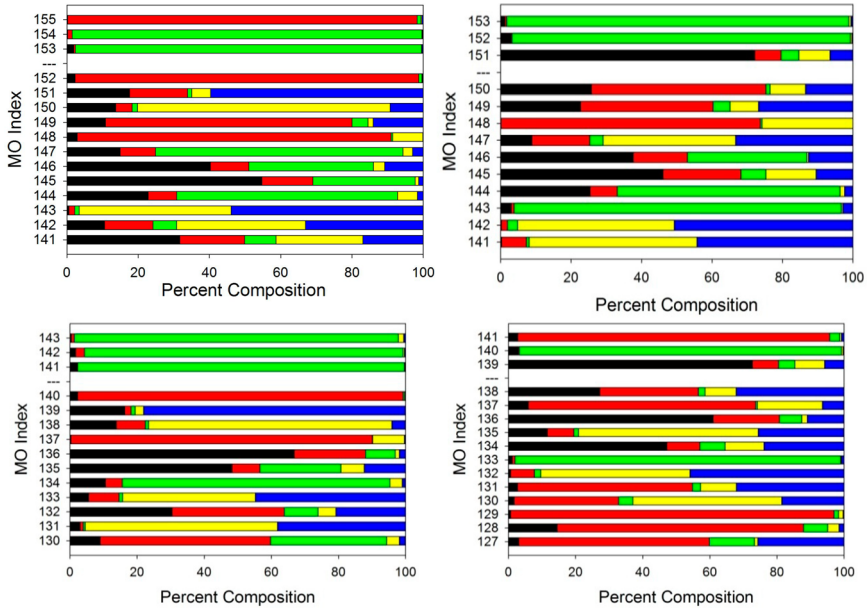

Figure 10. Percent contributions to the frontier molecular orbitals of species **I** (upper) and **III** (lower) in the lowest geometry-optimized ^{3}MLCT state (left) α-manifold and (right) β-manifold. Color code: ruthenium, black; α-diiminato(1-), red; α-diimine, green; longer-bonded [4-APy$_l$], blue; and shorter-bonded [4-APy$_s$], yellow. The HOMO−LUMO gap is identified by the white separator band ---. Data for species **II** and **IV** can be found in Supporting Information, Figure S14.

In the β-manifold, the β-LUMO, as anticipated, is mostly located on ruthenium, while in the frontier filled β-MOs there is rather more mixing between the two 4-APy ligands than in the α-manifold. The β−dσ* MOs are #149 and 151 lying more than 5.6 eV above the ^{3}MLCT β-HOMO.

The 4-APy$_l$ ligand lies at essentially the same distance from ruthenium in the ^{3}MLCT state as in the singlet ground state, while the 4-APy$_s$ ligand has a shorter Ru−N bond by ca. 0.03 to 0.04 Å.

The ^{3}MLCT state of the mono-CH_3CN species is also defined as a Ru^{III}(diimine)(diiminato) (4-APy)(CH_3CN)]$^{2+}$ species by the localized charge and spin data shown in Supporting Information, Table S9. The remaining 4-APy is perpendicular to the diiminato(1-) ligand (see Figure 9 (right)) in species **II·CH$_3$CN**, **III·CH$_3$CN**, and **IV·CH$_3$CN** but not in species **I·CH$_3$CN** where the acetonitrile group is perpendicular to diiminato. This leads to the supposition, albeit unproven, that it is the long bonded 4-APy$_l$ that is lost upon photolysis of **II**, **III**, and **IV**, a conclusion also reached by Sadler et al.[44] for the unsubstituted pyridine analogue of **III**. Further, as with the parent bis-4-APy species, the Ru−N(diiminato) bond (Supporting Information, Table S3) is shorter than the Ru−N(diimine) bond in these three complexes. However, in species **I·CH$_3$CN**, where the acetonitrile is perpendicular to diiminato, the Ru−N(diiminato) bonds are longer than the Ru−N(diimine) bonds. There is therefore a subtle difference between the equilibrium ^{3}MLCT states of **II**, **III**, and **IV** versus **I**, which may also contribute to the reason that species **I** loses both 4-APy ligands. However, the energy difference between species **I** with 4-APy perpendicular to diiminato and CH_3CN perpendicular to diiminato is probably not very large.

The lowest ^{3}MLCT state, which is photoactive, is not the same state as that involved in the most intense Ru 4dπ → π* LUMO (diimine) transition in the visible spectrum of the parent species (see Supporting Information, Tables S5−S8). There are many such possible transitions, arising from excitation of electrons from any of the three t_{2g} in O_h orbitals to the closely spaced LUMO and LUMO+1 MOs of the diimine ligands. This gives rise to the broadness of the visible band envelope (Figure 7).

Application of DFT to Understanding the Photolysis Data. The thermally equilibrated energy of the ^{3}MLCT state of [Ru^{III}(diimine)(diiminato)(4-APy)$_2$]$^{2+}$ was obtained by taking the ground state void conformation of species **I**−**IV**, rotating the 4-APy ligands into the over center conformation, and geometry-optimizing this configuration using S = 1 and unrestricted DFT. Subtracting the resulting self-consistent field (SCF) energy from the ground state, void SCF S = 0 energy, provides the relaxed energy of the lowest ^{3}MLCT state, relative to the ground state. This is shown in Figure 11.

Also shown in Figure 11 is the location of the peak of the experimental emission energies, which all occur just below the relaxed ^{3}MLCT energy as expected. In addition, in Figure 11, we locate the lowest energy Franck−Condon ^{1}MLCT, ^{3}MLCT, ^{1}MC, and ^{3}MC states (all void conformation). We also locate the positions of the exciting light at 420, 480, 520, and 580 nm.

The relevant MC states involve excitation of a 4dπ electron to a σ* MO that is antibonding between the metal and the departing ligand. There have been extensive studies of the role played by these metal centered π−σ* states in coupling to the lowest ^{3}MLCT state, thereby reducing its lifetime[22,30,37,40,42,46−50,53,65,68,95−97] and also providing a pathway for photolytic substitution of a ligand by solvent.[16,20] The lowest energy ^{3}MC state is commonly supposed, or calculated,[37,40,46,49] to lie in energy just *above* the ^{3}MLCT state and below the corresponding lowest ^{1}MLCT state. Thus photolysis may occur via intersystem crossing from a photoaccessible ^{1}MLCT state to the lower lying metal-centered π−σ* state or transfer to this state via higher vibrational levels of the ^{3}MLCT state.[10,15,30,35−41,46,48,98] Both Salassa[16,44] and Meyer[29] place the thermally equilibrated π−σ* ^{3}MC state *below* the lowest energy ^{3}MLCT state in *cis*-[Ru(bpy)$_2$(Py)$_2$]$^{2+}$. This was previously reported by Borg et al.[50b] and also confirmed by us, differing then from the 4-aminopyridine data. A range of

dx.doi.org/10.1021/ic5000205 | Inorg. Chem. 2014, 53, 3694−3708

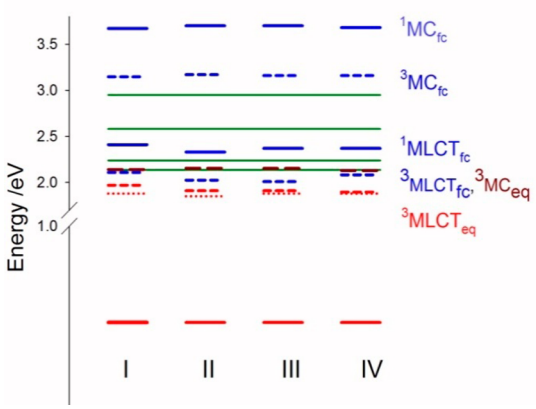

Figure 11. State and excitation energies relative to the spin singlet ground states of species **I**–**IV**. Thermally relaxed states are given in red (dark red for ^{3}MC states), and Franck–Condon states are in blue. Solid lines are singlets, and hatched lines are triplets. Experimental emission energies are red dotted lines. *Only the lowest energy example of a specific type of state is shown.* The horizontal green lines are the irradiation wavelengths for photolysis, 420, 480, 520, and 580 nm. Refer to text below for the existence of two relevant ^{3}MC optimized states that have almost the same energy. Thus the ^{3}MC identification actually refers to two states.

other ruthenium species, including $[Ru(bpy)_3]^{2+}$ are reported to possess ^{3}MC states lying *below* their lowest ^{3}MLCT state.[48,50−53,57,99]

We investigated the possible location of a *thermally equilibrated* ^{3}MC state by deriving the potential surface of the ^{3}MLCT state as a function of one Ru–N(4-APy) bond distance and looking for a new minimum associated with ^{3}MC (center conformation). Since the loss of the 4-Apy ligand is slow compared with thermal relaxation, it is justified to geometry-optimize along the reaction coordinate. Where ligand loss is ultrafast, on the femtosecond scale, it would not be justified.[47] Note also that as we weaken (lengthen) one Ru–N bond, a unique weaker field axis is established that, labeled as z, will stabilize the d_{z^2} orbital, bringing it closer in energy to the dπ orbitals, and hence will bring down the energy of d$\pi \rightarrow \sigma^*$ ^{3}MC states.[64]

A second minimum is observed (Figure 12) in the lowest spin triplet surfaces at a Ru–N(4-APy) distance of 2.8–2.9 Å in all four parent species and in their CH_3CN product surfaces (at 2.4–2.5 Å) (not shown), suggestive of a conical intersection[57] where a ^{3}MC state falls below the energy of the ^{3}MLCT state *at that Ru–N(4-APy) distance.* This procedure identifies a second minimum on the lowest triplet spin surface (as has been noted previously[16]), which should coincide approximately with the equilibrated minimum of the ^{3}MC state.

One may now use the structure obtained at the second minimum as *the starting geometry* of a new *unconstrained* optimization. This leads to the optimized ^{3}MC structures in which all vibrational frequencies are positive, confirming that the thermally equilibrated ^{3}MC structure, located in the second (local) minimum, has been identified. The resulting Ru–N(4-APy) distances (and SCF energies) (Table 6 and Supporting Information, Table S26) are extremely close to those observed at the minima shown in Figure 12. These thermally equilibrated ^{3}MC states lie about 1 eV below the location of the Franck–Condon ^{3}MC states (Figure 11). Note that in a real environment, these ^{3}MC states will be extremely short-lived

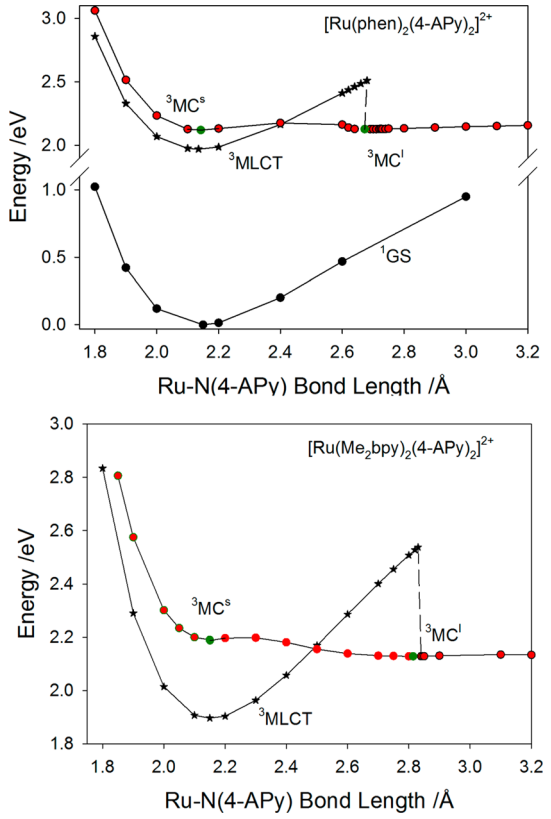

Figure 12. Energies (DFT, PCM CH_3CN) of ground, ^{1}GS, and lowest energy spin triplet state ^{3}MC surfaces as a function of one Ru–N(4-APy) bond length. The ^{3}MLCT (black stars) and ^{3}MC states (red circles) are identified along this surface. (top) $Ru(phen)_2(4\text{-}APy)(CH_3CN)]^{2+}$; (bottom) $Ru(Me_2bpy)_2(4\text{-}APy)_2]^{2+}$ (ground state omitted, is very similar to above data). See text for method of calculation. The green points locate the two thermally equilibrated ^{3}MC energy minima.

as a solvent molecule would displace the long bonded 4-APy ligand.

This ^{3}MC species is best described an intermediate spin ruthenium(II) species (Figure 13) in which occupation of the d_{z^2} orbital causes tetragonal distortion.[64] The long Ru–N(4-APy) bond along the z-axis is trans to an elongated Ru–N(diimine) pyridyl bond (ca. 2.4 Å). There are therefore two distinct diimine ligands, one in the tetragonal xy plane (in-plane diimine) and one perpendicular to this plane (axial diimine).

The triplet state potential energy surface was further explored by **starting with the optimized geometry of the ^{3}MC state** and systematically reoptimizing the structure with a successively *smaller* Ru–N(4-APy) frozen coordinate, that is, moving leftwards (in Figure 12) from the crossover near Ru–N(4-APy) = 2.8 Å toward the ^{3}MLCT minimum. The structure *does not cross back* to the ^{3}MLCT. It is evident that the calculation traces a very flat ^{3}MC surface back to smaller values of Ru–N(4-APy). Along this surface, the spin density on Ru(II) remains near 1.8, and the lowest energy harmonic frequency is very small *but positive.*

A closer look at the changes in geometry along this surface (Figure 14) reveals that there are at least two different ^{3}MC states. Near Ru–N(4-Apy) = 2.8 Å the ^{3}MC state is tetragonal (define xy in plane), with the z axis connecting the long Ru–N(4-APy) coordinate and the trans-located pyridyl nitrogen atom of the axial diimine ligand. However as Ru–N(4-Apy)

dx.doi.org/10.1021/ic5000205 | Inorg. Chem. 2014, 53, 3694−3708

Table 6. Selected Bond Lengths, Spin Density, And Energy Data for Optimized ^{3}MC States of the Parent Species

complex[a]	Ru−N(APy), Å	in-plane Ru−N(diimine), Å	axial Ru−N(diimine), Å	Ru spin density (charge)	^{3}MC SCF/Hartrees	ΔE, eV[c]
I (phen) ^{3}MC^l	2.44, 2.67[b]	2.12, 2.12	2.17, 2.44[b]	1.89 (0.90)	−1843.977 342 57	0.16
^{3}MC^s	2.14, 2.14	2.15, 2.52[b]	2.15, 2.51[b]	1.88 (0.85)	−1843.977 713 38	0.15
II (Ph_2ph)[d] ^{3}MC^l	2.15, 2.71[b]	2.11, 2.11	2.16, 2.42[b]	1.89 (0.89)	−2768.054 623 47	0.24
III (bpy) ^{3}MC^l	2.15, 2.79[b]	2.11, 2.11	2.16, 2.39[b]	1.89 (0.90)	−1691.536 155 90	0.24_5
^{3}MC^s	2.15, 2.14	2.12, 2.37[b]	2.23, 2.44[b]	1.81 (0.86)	−1691.534 570 69	0.29
IV (Me_2bpy) ^{3}MC^l	2.15, 2.81[b]	2.10, 2.10	$2.16, 2.39_5$[b]	1.89 (0.89)	−1848.794 676 81	0.23
^{3}MC^s	2.15, 2.14	2.12, 2.37[b]	2.23, 2.45[b]	1.82 (0.85)	−1848.792 503 51	0.29

[a]See Supporting Information, Table S26 for the monoacetonitrile species. [b]This ligand is lying along the axis of elongation. [c]The ^{3}MC energy, relative to the lowest ^{3}MLCT equilibrium energy. [d]The ^{3}MC^s data not derived.

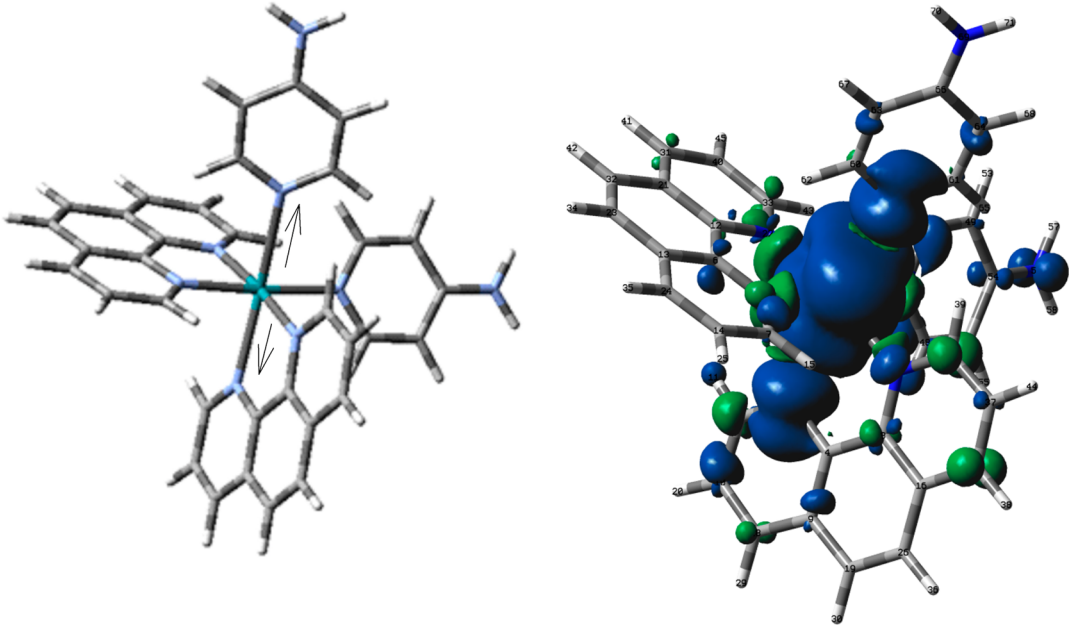

Figure 13. The ^{3}MC^l thermally equilibrated $[Ru(phen)_2(4\text{-}APy)_2]^{2+}$ state; (left) skeleton geometry, with long, *z*-axis pointing up (indicated by arrows); (right) spin density. Solvent (CH_3CN) PCM DFT calculation. In both cases the long bonded Ru−N(4-APy) ligand points to the top of the figure.

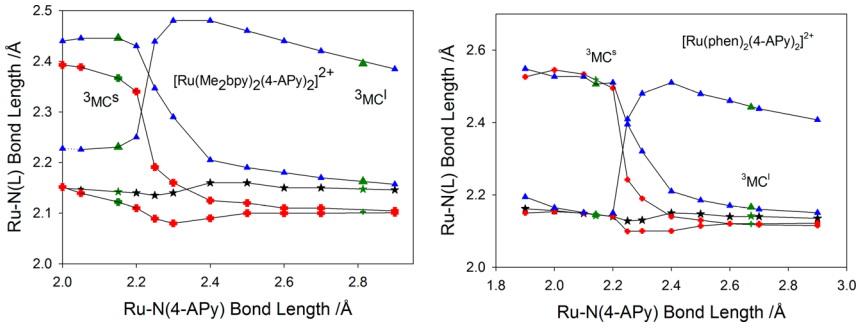

Figure 14. Variation in skeletal ruthenium ligand bond lengths, in ^{3}MC states, as a function of one Ru−N(4-APy) bond length. DFT, PCM calculation, see text for method. Bond distances are indicated as follows: the other Ru−N(4-APy), black stars; the two Ru−N bonds to the in-plane diimine, red crosses; the two Ru−N bonds to the axial-diimine, blue triangles. The green data points identify the relevant bond distances at the minima of the two optimized ^{3}MC states. See text for definition of in-plane and axial diimines.

decreases, the *z*-axis rotates to lie between two pyridyl nitrogen atoms each from a different diimine ligand. This is clearly a different ^{3}MC state from the one existing near Ru−N(4-APy) = 2.8 Å. We henceforth refer to the long Ru−N(4-APy) state near 2.8 Å as ^{3}MC^l (long bonded ^{3}MC state) and the trans diimine state near Ru−N(4-APy) = 2.2 Å as ^{3}MC^s (short bonded ^{3}MC state). Between these two limits there is a mixed configuration. It proved possible to geometry-optimize ^{3}MC^s with no constraints, (all positive harmonic frequencies), and the locations of both ^{3}MC states are shown by the green symbols in Figures 12 and 14. They occupy local shallow minima. Occupation of ^{3}MC^s is not likely to lead to loss of 4-aminopyridine. The geometry of the ^{3}MC^s state is very similar[46] to the lowest ^{3}MC state of species such as $[Ru(bpy)_3]^{2+}$.

To explore the ^{3}MC surface at Ru−N(4-APy) < 2.2 Å, it is appropriate to start from the ^{3}MC^s geometry and freeze the

dx.doi.org/10.1021/ic5000205 | Inorg. Chem. 2014, 53, 3694−3708

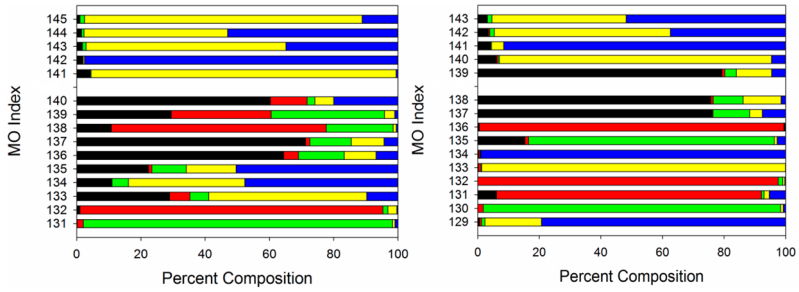

Figure 15. Percentage contributions to the frontier MOs of species **III** in its lowest energy, geometry-optimized ^{3}MC^l state (left, α-manifold; right, β-manifold). Ruthenium, black; [4-APy$_l$], red; and [4-APy$_s$], green; in-plane short bonded bpy, yellow; axial longer bonded bpy, blue.

Ru−N(4-APy) coordinate, with the results shown in Figure 12. The rising left-hand wing of the ^{3}MC^s state does not cross back to ^{3}MLCT within the studied region of the triplet surface.

The existence of this hitherto unexplored flat ^{3}MC surface (a component of the overall 3-dimensional surface) extending from Ru−N(4-APy) ≈ 1.8 to >3.0 Å has profound importance with respect to the photosolvation mechanism. Once the ^{3}MLCT state is accessed, either by intersystem crossing from higher states or by direct excitation with low energy light, it must require very little energy to access the ^{3}MC^s state. Essentially no energy is then required to move to the ^{3}MC^l state, followed by dissociation. Direct access to ^{3}MC^l via the ^{3}MLCT is not required.

Table 6 (and Supporting Information, Table S26) reveals that the ^{3}MC^l states lie about 0.2 eV above the equilibrated ^{3}MLCT state except for the photoactive [Ru(phen)$_2$(4-APy)(CH$_3$CN)]$^{2+}$ (**I·CH$_3$CN**) where the ^{3}MLCT and ^{3}MC states are almost degenerate. The ground state energy rises with increasing Ru−N(4-APy) distance, and the energy gap between the ^{3}MC^l state and the ground state at the crossover Ru−N(4-APy) distance is fairly small, for example, 0.7 eV for [Ru(Me$_2$bpy)$_2$(4-APy)$_2$]$^{2+}$. This then likely provides an easy mechanism for nonradiative decay of the ^{3}MC^l state to the ground state, and contributes to a small photosolvolysis quantum yield. The small gap also provides indirect confirmation that the observed emission stems from the ^{3}MLCT state and not from the ^{3}MC state.

We comment briefly on the electronic structures of these ^{3}MC^l states. The α-LUMO and α-LUMO+1 (species **III**, Figure 15) are essentially localized on the in-plane and axial diimines, respectively. The β-LUMO is almost a pure d-orbital, revealing the dπ-orbital, coupled to the in-plane diimine, from which electron excitation occurs to create this ^{3}MC state. There are deeper-lying orbitals in both manifolds that lie almost exclusively on one or the other of the 4-APy ligands.

Natural population charges and spin densities on ruthenium, from the NBO6 program,[100] for the states of interest are shown in Supporting Information, Table S4 (for comparison with the Mulliken data in Table 6). For example, for species **III**, the NBO spin density in the ^{3}MLCT state lies 0.85 on Ru(III) and 1.03 on the ligands, primarily on one bpy ligand as noted above. For the same species, the spin density in the ^{3}MC^l state is 1.78 on ruthenium, in agreement with the formulation as tetragonal Ru(II). There is little overlap between the d_{z^2} orbital and the rest of the molecule and essentially no spin density anywhere in the rest of the molecule except for the two nitrogen atoms which overlap d_{z^2}. These values are similar to those reported in previous studies of the ^{3}MC states of [Ru(bpy)$_3$]$^{2+}$, [Ru(Pz)$_2$(NH$_3$)$_4$]$^{2+}$, and related species.[16,46,49,50,99]

The mixing of excited states in photochemical processes has been addressed for a long time.[48,99,101−105] Previous workers have suggested that, in these systems, configurational interaction between ^{3}MLCT and ^{3}MC causes the Ru−N bond to elongate.[16,20] Such mixing has been previously suggested to cause distortion in the ^{3}MLCT state.[66,106]

There will be some configurational interaction between the diabatic ^{3}MLCT and ^{3}MC states, given the low symmetry of these species and their close energy. Such mixing may be the cause of the elongation of one Ru−N(4-APy) bond in the ^{3}MLCT state.

The question that can be addressed is whether the further elongation of the Ru−N(4-APy) bond is accompanied by an *additional* admixture of ^{3}MC^l into ^{3}MLCT. The data appear not to support such an additional contribution in these systems that ignore vibrational mixing and spin−orbit coupling at this level of approximation. Thus if the initial ^{3}MLCT state is compared with ^{3}MC^l we note, of course, that the spin density on the ruthenium is increased in the ^{3}MC^l state and that there is elongation not only of the Ru−N(4-APy) coordinate but also of the Ru−N(diimine) coordinate trans to it. If a structure is considered, intermediate between ^{3}MLCT and ^{3}MC^l, just before the crossover, specifically at a Ru−N(4-APy) distance of 2.75 Å (species **III**), this might be expected to demonstrate a 4d configuration, closer to that of ^{3}MC, if the ^{3}MLCT and ^{3}MC^l states are additionally mixed. However, the total spin density on Ru at this distance is still 0.90, unchanged from the pure ^{3}MLCT (Ru−N(4-APy) (2.15 Å) state. Further, the Ru−N(bpy) distance trans to the long Ru−N(4-APy) bond is 2.02 Å, 2.07 Å in the ^{3}MLCT state, and much shorter than the 2.43 Å in the ^{3}MC^l state. This argues for no significant *additional* mixing of ^{3}MLCT with ^{3}MC^l along the long reaction coordinate (Figure 12).

The extent of configurational interaction between the ^{3}MC^l state and ^{3}MLCT states can also be addressed at the equilibrium configuration of the ^{3}MC^l state. This is relatively easy to assess since a pure ^{3}MC state, in the absence of π-back-donation, would have no occupation of the π^* lowest unoccupied fragment orbital (LUFO) and LUFO+1 of the diimine ligands. These orbitals can mix with filled 4d orbitals of Ru and thereby become partially occupied. Using the AOMIX family of software (see Experimental Section) the occupation of these orbitals can be directly discerned. Any partial occupation of the LUFO and LUFO+1 of the diimines can be explained as π-back-donation from Ru^{II}. This, however, is conceptually identical with saying that Ru^{III}(diiminato) excited states, ^{3}MLCT states, are mixed into the ^{3}MC state. Thus any occupation of LUFO, LUFO+1 is an indicator of configurational mixing of the ^{3}MC state likely with several different

dx.doi.org/10.1021/ic5000205 | Inorg. Chem. 2014, 53, 3694−3708

^{3}MLCT states. In fact, this occupation is quite small, of the order of 0.03−0.06 electrons (total over both MOs) in each of the α- and β-manifolds. Thus, there is some configurational mixing of these states, but it is not especially significant.

Also of interest are the low-lying excited states of the ^{3}MC^l state, obtained via TD-DFT calculation. The ^{3}MLCT state, which is the lowest triplet charge transfer state in the ground state geometry, becomes the third excited state (for species **I** and **III**) of the ^{3}MC^l geometry, lying ca. 1.4 eV above the ^{3}MC^l state. The two intervening states are also ^{3}MC (d−d) (Supporting Information, Table S25).

CONCLUSION

Two conformations of the 4-APy ligands are recognized, the so-called void and over center conformations, and there appears to be a change in the thermodynamically favored state from the void conformation in the ground state to the over center conformation in the lowest ^{3}MLCT state.

Further evidence is presented to show that a ^{3}MC state is involved in the photolysis of these bis-diimine species. Excitation spectra and quantum yields reveal that these states are very efficiently populated even at longer wavelength where there is very little direct absorption. Local minima are revealed showing ^{3}MC^l states lying at energies just greater than the equilibrium energy of the ^{3}MLCT state but well below the energy of the Franck−Condon ^{3}MLCT, at the extended Ru−N(4-APy) distance.

With respect to the mechanism by which the ^{3}MC state is populated, the previous understanding has been that, with high energy excitation, intersystem crossing will occur from ^{1}MLCT to ^{3}MLCT crossing over to ^{3}MC via higher vibrational states of ^{3}MLCT. Here we have demonstrated the existence of a second ^{3}MC state that can easily be accessed both via intersystem crossing and thermally and that can lead to the photodissociative ^{3}MC^l state with essentially no further input of energy.

The low energy excitation at 580 nm is sufficient to populate the ^{3}MLCT state directly (see Figure 11). Despite the low absorption probability at this wavelength, it is indeed likely that the photosolvolysis mechanism is access of ^{3}MC^s leading directly to ^{3}MC^l.

The low quantum yields observed for these photosolvolyses arise from competition between emission and nonradiative decay from ^{3}MLCT and the ensuing thermal population of ^{3}MC, which can then nonradiatively decay to the relatively nearby ground state or undergo solvolysis. There appears to be no simple pathway to cross back to ^{3}MLCT.

EXPERIMENTAL SECTION

Optical spectra were recorded on an Agilent 8453 UV−vis spectrophotometer. ^{1}H NMR spectra were measured in a CD_3CN solution using a Bruker DRX-400 or DRX-500 spectrometer. All chemical shifts (δ) are given in ppm with reference to the hydrogen signal of the methyl group of tetramethylsilane (TMS) as internal standard, and the coupling constants (J) are in Hz. C, H, N elemental analyses were performed on an EA 1110 CHNS-O Carlo Erba Instrument in the Microanalytical Laboratory at Universidade Federal de São Carlos (UFSCar). The HPLC system consisted of a Shimadzu liquid chromatograph equipped with a Waters Model 6000A pump, SPD-10AV UV−vis detector. An ODS column (5 μm; 150 mm × 4.6 mm i.d.; 100 Å; Phenomenex RP-18) was used in all experiments. Isocratic elution with a 50:50 mixture of CH_3CN/H_2O containing 0.01% hexafluorothioacetone (HFTA), pH 3.0, was used at constant flow rate of 0.3 mL min^{-1}, at room temperature. Samples for analysis were dissolved in CH_3CN; measured (20 μL) volumes were injected throughout the experiments and monitored at λ_{max} absorption. Electrochemical measurements were recorded using a μAutolab Type III potentiostat. Acetonitrile solutions typically contained 1.0 × 10^{-3} mol L^{-1} of the complex. A platinum disk served as the working (d = 0.2 mm) and counter (d = 0.5 mm) electrode, and Ag^+/Ag wire was used as the reference electrode. Solutions contained 0.1 M tetra-*n*-butylammonium hexafluorophosphate ($TBAPF_6$) as supporting electrolyte. Data were internally calibrated by reference to the ferrocene couple,[107] assumed to lie at 0.44 V versus the AgCl/Ag couple.

Photosubstitution Quantum Yield Determinations. Solutions (3.5 mL) of complexes **I**−**IV** (∼1 × 10^{-4} mol L^{-1}) were rigorously deoxygenated using super N_2 atmosphere and then irradiated with a 300 W Xenon lamp (model 6258) in a Newport Oriel Product Line, model 69911 Universal Arc Lamp Power Supply source selected with an appropriate interference filter (Oriel) (420, 480, 520, and 580 nm) and using a 1 cm path length, four clear-sided, quartz cell. The progress of the photoreaction was monitored by UV−vis spectroscopy. During photolysis the solution in the cell was irradiated for defined time periods. The samples were rapidly stirred to ensure a uniform absorption throughout the cell. To avoid flash photolysis of secondary products, fresh solutions of complexes were flashed once (one transient trace taken), and then the solution was replaced by a new one.

The light intensity was determined by chemical actinometry measurements using ferric oxalate solution for irradiation wavelengths at 420 and 480 nm and Reinecke's salt solution for irradiation wavelengths at 520 and 580 nm.[107,108] The photoreactions were monitored by UV−vis, emission, HPLC, and ^{1}H NMR spectroscopic techniques and by cyclic voltammetry; UV−vis spectra were also recorded for solutions kept in the dark to assess the possibility of thermal processes. No solvolysis occurs in the dark. Absorption at wavelengths of 370, 380, 400, 420, 440, 460, 480, 500, 520, and 540 nm for all complexes was monitored for quantum yield (ϕ) determination (first 10% of the reaction) using eq 3. All reported ϕ numbers are the average of two independent experiments, and the error is the standard deviation. The irradiation wavelengths chosen were 420, 480, 520, and 580 nm.

$$\phi = \frac{\Delta \mathrm{Abs} V}{I_0 f \Delta t \Delta \varepsilon} \tag{3}$$

where ΔAbs = range of absorbance at monitoring wavelength, V = volume of irradiated sample, I_0 = light intensity at irradiation wavelength (in einstein s^{-1}), and f = the fraction of light absorbed at irradiation wavelength. Function f is derived from eq 4.

$$\log(1 - f) = [-(\mathrm{Abs}_{t=2} + \mathrm{Abs}_{t=2})/2] \tag{4}$$

where Δt = range of irradiation time (in seconds) and $\Delta\varepsilon$ = difference in molar absorptivity between reactant and product at monitoring wavelength.

Time-Resolved Optical Spectra. These spectra were obtained using a laser flash-photolysis apparatus containing a Continuum Q-switched Nd:YAG laser (Continuum, Santa Clara, CA) with excitation provided by the third harmonic at λ = 35 emit 5 nm. The pulse length was 8 ns, the beam diameter incident on sample was 6 mm, and the repetition rate was 10 Hz. Optical spectra were recorded 10 ns after the pulse. The laser pulse was set up to 8 mJ per pulse in the photobleaching studies measured with a Field Master power meter with L-30 V head. The growth−decay kinetics were measured at a single wavelength using a monochromator (M300 from Bentham) and a photomultiplier (Hamamatsu, model R928P). Transient decays were averaged using a Tetronix TDS 340A digital oscilloscope. Digitized kinetics data were transferred to a personal computer (PC) for analysis with software supplied by Edinburgh Instruments. The optical spectra of the solutions following these experiments were identical to the initial solutions, within experimental error.

Luminescence Spectra. These spectra were obtained on a Shimadzu RF-5301PC fluorescence spectrophotometer. Solutions

dx.doi.org/10.1021/ic5000205 | Inorg. Chem. 2014, 53, 3694−3708

(10^{-6} mol L^{-1}; $A\lambda_{max} < 0.1$) of the complexes in the appropriated solvent were used. The solutions were deaerated by bubbling with high-purity nitrogen for at least 40 min.

Fluorescence Emission Decay. The time-correlated single-photon counting (TCSP) method was used to obtain fluorescence emission decay curves.[109] The excitation source was a Tsunami 3950 (Spectra Physics) titanium-sapphire laser, pumped by a solid-state Millenia Xs (Spectra Physics) laser. The repetition rate of the 5 ps pulses was set to 800 kHz using the pulse picker Spectra Physics 3980. The laser was tuned to give output at 945 nm, and a second harmonic generator LBO crystal (GWN-23PL Spectra Physics) gave the 472 nm excitation pulses that were directed to an Edinburgh FL900 spectrometer, where the L-format configuration allowed the detection of the emission at right angle from the excitation. The emission wavelength was selected by a monochromator, and emitted photons were detected by a refrigerated Hamamatsu R3809U microchannel plate photomultiplier. The full width at half-maximum (fwhm) of the instrument response function was typically 2.20 ns, and measurements were made using time resolution of 0.245 ns per channel. F900 software provided by Edinburgh Instruments was used to analyze the decay curves, and the adequacy of the multiexponential decay fitting was judged by inspection of the plots of weighted residuals and by statistical parameters such as reduced chi-square.

Materials. All solvents used in synthetic work were of HPLC grade. Deuterated solvents were purchased from Aldrich. $RuCl_3 \cdot 3H_2O$, 1,10-phenanthroline (phen), 4,7-diphenyl-1,10-phenanthroline (Ph_2phen), 2,2′-bipyridine (bpy), 4,4′-dimethyl-2,2′-bipyridine (Me_2bpy), 4-aminopyridine (4-APy), lithium chloride (LiCl), ammonium hexafluorophosphate (NH_4PF_6), tetrabutylammonium hexafluorophosphate ($TBAPF_6$), and HPF_6 were purchased from Sigma-Aldrich.

Synthesis of Complexes. All reactions were performed under nitrogen atmosphere. The starting materials, *cis*-[Ru(α-diimine)$_2$(OH_2)$_2$](PF_6)$_2$·H_2O or *cis*-[Ru(α-diimine)Cl_2]$^{2+}$, were prepared according to literature methods.[58,59,65] The *cis*-[Ru(α-diimine)$_2$(4-APy)$_2$](PF_6)$_2$ complexes were synthesized from the corresponding *cis*-[Ru(α-diimine)$_2$(OH_2)$_2$](PF_6)$_2$ by reaction of the latter with 4-aminopyridine in ethanol/water mixture. A representative case is detailed below.

(a) cis-[Ru(phen)$_2$(4-APy)$_2$](PF$_6$)$_2$·2H$_2$O (I). *cis*-[Ru(phen)$_2$(OH_2)$_2$](PF_6)$_2$ (51 mg, 0.063 mmol) was dissolved in a 1:1 EtOH/H_2O mixture (10 mL), and 4-APy (13.7 mg, 0.15 mmol) ligand was added. The solution was stirred under nitrogen atmosphere for 8 h under reflux. A stoichiometric amount of NH_4PF_6 was added to precipitate the complex. The precipitate was redissolved in a minimum amount of MeOH and chromatographed on a Sephadex LH-20 column (2.5 × 50 cm) using MeOH and toluene (3:1 v/v) as eluant. The red band was collected, and the solvent was removed on a rotary evaporator. The solid so obtained was dissolved in MeOH, and the solution was dropped into diethyl ether. The dark red precipitate was filtered, washed with water, ethanol and diethyl ether, and dried under vacuum. Yield: 44 mg, 71%. ^{1}H NMR (CD_3CN): δ 9.35 (H2, dd), 8.67 (H4, dd), 8.32 (H7, dd), 8.15 (H5, d), 8.09 (H3, m), 8.05 (H6, d), 7.94 (H9, dd), 7.76 (Hα,α′, d), 7.42 (H8, m), 6.34 (Hβ,β′, d), 5.26 (N−H (NH_2), s) ppm. Cyclic voltammetry: $E_{1/2}$ = 1.00 V versus saturated calomel electrode (SCE). Anal. Calcd. for $RuC_{34}H_{32}N_8P_2F_{12}O_2$: C, 41.80; H, 3.30; N, 11.48. Found: C, 41.7; H, 3.13; N, 11.5%.

(b) cis-[Ru(Ph$_2$phen)$_2$(4-APy)$_2$](PF$_6$)$_2$·2H$_2$O (II). Complex **II** was obtained from *cis*-[$RuCl_2$(Ph_2phen)$_2$]$^{2+}$ in 68% yield after 8 h of reflux. ^{1}H NMR (CD_3CN): δ 9.47 (H2, d), 7.69 (H4, m), 7.69 (H7, m), 8.15 (H5, d), 8.16 (H3, m), 8.06 (H6, d), 8.10 (H9, d), 7.94 (Hα,α′, d), 7.48 (H8, m), 6.47 (Hβ,β′, d), 5.35 (N−H (NH_2), s) ppm. Cyclic voltammetry: $E_{1/2}$ = 0.98 V versus SCE. Anal. Calcd. for $RuC_{58}H_{48}N_8P_2F_{12}O_2$: C, 54.42; H, 3.78; N, 8.75. Found: C, 54.11; H, 3.88; N, 8.40%.

(c) cis-[Ru(bpy)$_2$(4-APy)$_2$](PF$_6$)$_2$·2H$_2$O (III). Complex **III** was obtained from *cis*-[Ru(bpy)$_2$(O H_2)$_2$]$^{2+}$ in 81% yield after 8 h of reflux. ^{1}H NMR (CD_3CN): δ 8.92 (H2, d), 8.08 (H4, m), 7.72 (H7, m), 7.85 (H5, d), 8.34 (H3, d), 7.85 (H6, m), 7.84 (H9, m), 7.63 (Hα,α′, dd), 8.25 (H8, d), 6.40 (Hβ,β′, dd), 5.32 (N−H (NH_2), s) ppm. Cyclic voltammetry: $E_{1/2}$ = 0.92 V versus SCE. Anal. Calcd. for $RuC_{30}H_{32}N_8P_2F_{12}O_2$: C, 38.84; H, 3.48; N, 12.08. Found: C, 38.70; H, 3.54; N, 11.80%.

(d) cis-[Ru(Me$_2$bpy)$_2$(4-APy)$_2$](PF$_6$)$_2$·2H$_2$O (IV). Complex **IV** was obtained from *cis*-[Ru(Me_2bpy)$_2$(OH_2)$_2$]$^{2+}$ in 82% yield after 8 h of reflux. ^{1}H NMR (CD_3CN): δ 8.71 (H2, d), 2.58 (H4, s), 2.42 (H7, s), 8.20 (H5, s), 7.54 (H3, d), 8.10 (H6, s), 7.64 (H9, d), 7.63 (Hα,α′, dd), 7.11 (H8, d), 6.39 (Hβ,β′, dd), 5.30 (N−H (NH_2), s) ppm. Cyclic voltammetry: $E_{1/2}$ = 0.85 V versus SCE. Anal. Calcd. for $RuC_{34}H_{40}N_8P_2F_{12}O_2$: C, 41.51; H, 4.10; N, 11.39. Found: C, 41.56; H, 4.20;N, 11.30%.

COMPUTATIONAL DETAILS

Geometry-optimized structures were obtained using Gaussian 09, Revision B.01,C.01, D.01,[110] employing density functional theory (DFT) calculations, using the hybrid B3LYP exchange-correlation functional[111] and the LanL2DZ basis.[112−115] The solvent (acetonitrile) was included using the polarized continuum model (PCM).[80,81] A tight convergence (10^{-8} au) was used for all DFT calculations. Vibrational frequency calculations were performed on all optimized complexes to verify that an energy minimum had been attained. The wave functions were also checked for stability. All the ground states are spin singlets. The energies of the predicted electronic transitions were obtained via the time-dependent DFT (TD-DFT) method.[39,116,117] The absorption profiles of the complexes were calculated using the SWIZARD program.[118] Extended charge decomposition analysis (ECDA) was carried out employing the AOMIX-CDA program.[119] The natural bond orbital calculation was performed using the NBO6 program[92] patched into GO9 vD.01. Optimized ^{3}MC states were obtained starting from variously defined geometries as noted in the text.

ASSOCIATED CONTENT

Supporting Information

Detailed DFT data, *xyz* coordinates of ground and excited ^{3}MLCT species, DFT-optimized bond lengths, optical assignments, NMR, electrochemical, emission, and photolysis data are provided. This material is available free of charge via the Internet at http://pubs.acs.org.

AUTHOR INFORMATION

Corresponding Authors

*E-mail: rosem@ufscar.br (R.M.C.).
*E-mail: blever@yorku.ca (A.B.P.L.).

Notes

The authors declare no competing financial interest.

ACKNOWLEDGMENTS

We thank the Natural Sciences and Engineering Research Council (Ottawa) for financial support (to A.B.P.L.) and FAPESP (Proc. 2006/50322-0, 2008/52859-7 and 2009/08218-0) to M.R.C., C.R.C., and R.M.C. Computational work was made possible by the facilities of the Shared Hierarchical Academic Research Computing Network, Ontario, Canada (http://www.sharcnet.ca). We also thank Dr. Elaine S. Dodsworth, Profs. Serge Gorelsky and Antonin Vlĉek for useful discussions, and Profs. Amando S. Ito and Antonio C. Tedesco (FFCL/RP-USP) for emission lifetime and transient absorption spectrum measurements.

REFERENCES

(1) Stochel, G.; Wanat, A.; Kulís, E.; Stasicka, Z. *Coord. Chem. Rev.* **1998**, *171*, 203−220.

(2) Carlos, R. M.; Cardoso, D. R.; Castellano, E. E.; Osti, R. Z.; Camargo, A. J.; Macedo, L. G.; Franco, D. W. *J. Am. Chem. Soc.* **2004**, *126*, 2546−55.

(3) Salierno, M.; Marceca, E.; Peterka, D. S.; Yuste, R.; Etchenique, R. *J. Inorg. Biochem.* **2010**, *104*, 418−22.
(4) Salierno, M.; Fameli, C.; Etchenique, R. *Eur. J. Inorg. Chem.* **2008**, 11125−28.
(5) Zayat, L.; Noval, M. G.; Campi, J.; Calero, C. I.; Calvo, D. J.; Etchenique, R. *ChemBioChem* **2007**, *8*, 2035−38.
(6) Brindell, M.; Kulis, E.; Elmroth, S. K. C.; Urbanska, K.; Stochel, G. *J. Med. Chem.* **2005**, *48*, 7298−04.
(7) Inglez, S. D.; Lima, F. C. A.; Camilo, M. R.; Daniel, J. F. S.; Santos, E. D. A.; Lima-Neto, B. S.; Carlos, R. M. *J. Braz. Chem. Soc.* **2010**, *21*, 157−168.
(8) Zayat, L.; Calero, C.; Albores, P.; Baraldo, L.; Etchenique, R. *J. Am. Chem. Soc.* **2003**, *125*, 882−883.
(9) Cardoso, C. R.; de Aguiar, I.; Camilo, M. R.; Lima, M. V. S.; Ito, A. S.; Baptista, M. S.; Pavani, C.; Venâncio, T.; Carlos, R. M. *Dalton Trans.* **2012**, *41*, 6726−34.
(10) Ragazzon, G.; Bratsos, I.; Alessio, E.; Salassa, L.; Habtemariam, A.; McQuitty, R. J.; Clarkson, G. J.; Sadler, P. J. *Inorg. Chim. Acta* **2012**, *393*, 230−238.
(11) Barragan, F.; Lopez-Senin, P.; Salassa, L.; Betanzos-Lara, S.; Habtemariam, A.; Moreno, V.; Sadler, P. J.; Marchan, V. *J. Am. Chem. Soc.* **2011**, *133*, 14098−14108.
(12) Higgins, S. L. H.; Brewer, K. J. *Angew. Chem., Int. Ed* **2012**, *51*, 11420.
(13) Howerton, B. S.; Heidar, D. K.; Glazer, E. C. *J. Am. Chem. Soc.* **2012**, *134*, 8324.
(14) Liu, Y.; Turner, D. B.; Singh, T. N.; Angeles-Boza, A. M.; Chouai, A.; Dunbar, K. R.; Turro, C. *J. Am. Chem. Soc.* **2009**, *131*, 26−7.
(15) Garner, R. N.; Joyce, L. E.; Turro, C. *Inorg. Chem* **2011**, *50*, 4384−91.
(16) Salassa, L.; Garino, C.; Salassa, G.; Gobetto, R.; Nervi, C. *J. Am. Chem. Soc.* **2008**, *130*, 9590−9597.
(17) Salassa, L.; Borfecchia, E.; Ruiu, T.; Garino, C.; Gianolio, D.; Gobetto, R.; Sadler, P. J.; Cammarata, M.; Wulff, M.; Lamberti, C. *Inorg. Chem.* **2010**, *49*, 11240−11248.
(18) Zayat, L.; Salierno, M.; Etchenique, R. *Inorg. Chem.* **2006**, *45*, 1728−1731.
(19) Salassa, L.; Gianolio, D.; Garino, C.; Salassa, G. B.; Ruiu, T.; Nervi, C.; Gobetto, R.; Bizzarri, R.; Sadler, P. J.; Lamberti, C. *J. Phys.: Conf. Ser.* **2009**, *190*, 012141.
(20) Salassa, L. G. C.; Salassa, G.; Nervi, C.; Gobetto, R.; Lamberti, C.; Gianolio, D.; Bizzarri, R.; Sadler, P. J. *Inorg. Chem.* **2009**, *48*, 1469−1481.
(21) Nikolenko, V.; Yuste, R.; Zayat, L.; Baraldo, L. M.; Etchenique, R. *Chem.Commun.* **2005**, 1752.
(22) Garino, C.; Salassa, L. *Philos. Trans. Roy. Soc. London* **2013**, *371*, 20120134.
(23) Garino, C.; Gobetto, R.; Nervi, C.; Salassa, L.; Rosenberg, E.; Ross, J. B. A.; Chu, X.; Hardcastle, K. I.; Sabatini, C. *Inorg. Chem.* **2007**, *46*, 8752−8762.
(24) (a) Ershov, A. Yu.; Shashko, A. D.; Sizova, O. V.; Ivanova, N. V.; Burov, S. V.; Kuteikina-Teplyakova, A. V. *Russ. J. Gen. Chem.* **2003**, *73*, 135−140. (b) Sizova, O. V.; Ershov, A. Yu.; Ivanova, N. V.; Shashko, A. D.; Kuteikina-Teplyakova, A. V. *Russ. J. Coord. Chem.* **2003**, *29*, 494−500.
(25) Wacholtz, W. F.; Auerbach, R. A.; Schmehl, R. H. *Inorg. Chem.* **1986**, *25*, 227−234.
(26) Inglez, S. D.; Lima, F. C. A.; Silva, A. B. F.; Simioni, A. R.; Tedesco, A. C.; Daniel, J. F. S.; Lima-Neto, B. S.; Carlos, R. M. *Inorg. Chem.* **2007**, *46*, 5744−5753.
(27) Suen, H. F.; Wilson, S. W.; Pomerantz, M.; Walsh, J. L. *Inorg. Chem.* **1989**, *28*, 786−791.
(28) (a) Van Houten, J.; Watts, R. J. *J. Am. Chem. Soc.* **1976**, *98*, 4853. (b) Van Houten, J.; Watts, R. J. *Inorg. Chem.* **1978**, *17*, 3381−85.
(29) Durham, B.; Caspar, J. V.; Nagle, J. K.; Meyer, T. J. *J. Am. Chem. Soc.* **1982**, *104*, 4803.
(30) Sauvage, J.-P.; Collin, J.-P.; Chambron, J.-C.; Guillerez, S.; Coudret, C.; Balzani, V.; Barigelletti, F.; De Cola, L.; Flamigni, L. *Chem. Rev.* **1994**, *94*, 993−1019.
(31) Caspar, J. V.; Meyer, T. J. *J. Am. Chem. Soc.* **1983**, *105*, 5583−90.
(32) Barigelletti, F.; Juris, A.; Balzani, V.; Belser, P.; Von Zelewsky, A. *J. Phys. Chem.* **1987**, *91*, 1095−1098.
(33) Wagenknecht, P. S.; Ford, P. C. *Coord. Chem. Rev.* **2011**, *255*, 591−616.
(34) Adelt, M.; Devenney, M.; Meyer, T. J.; Thompson, D. W.; Treadway, J. A. *Inorg. Chem.* **1998**, *37*, 2616−17.
(35) Rillema, D. P.; Blanton, C. B.; Shaver, R. J.; Jackman, D. C.; Boldaji, M.; Bundy, S.; Worl, L. A.; Meyer, T. J. *Inorg. Chem* **1992**, *31*, 1600−1606.
(36) (a) Malouf, G.; Ford, P. C. *J. Am. Chem. Soc.* **1977**, *99*, 7213−22. (b) Ford, P. C.; Wink, D.; Dibenedetto, J. *Prog. Inorg. Chem.* **1983**, *30*, 211.
(37) De Cola, L.; Barigelletti, F.; Cook, M. J. *Helv. Chim. Acta* **1988**, *71*, 733−41.
(38) da Silva, R. S.; Gorelsky, S. I.; Dodsworth, E. S.; Tfouni, E.; Lever, A. B. P. *J. Chem. Soc., Dalton Trans.* **2000**, 4078−4088.
(39) Vlĉek, A.; Zalis, S. *Coord. Chem. Rev.* **2007**, *251*, 258−287.
(40) Petroni, A.; Slep, L. D.; Etchenique, R. *Inorg. Chem.* **2008**, *47*, 951−6.
(41) Sizova, O. V.; Inanova, N. V.; Ershov, A. Yu.; Shashko, A. D. *Russ. J. Gen. Chem.* **2003**, *73*, 1846.
(42) Winkler, J. R.; Netzel, T. L.; Creutz, C.; Sutin, N. *J. Am. Chem. Soc.* **1987**, *109*, 2381−92.
(43) Wacholtz, W. M.; Auerbach, R. A.; Schmehl, R. H.; Ollino, M.; Cherry, W. R. *Inorg. Chem.* **1985**, *24*, 1758−1760.
(44) Borfecchia, E.; Garino, C.; Salassa, L.; Ruiu, T.; Gianolio, D.; Zhang, X.; Attenkofer, K.; Chen, L. X.; Gobetto, R.; Sadler, P. J.; Carlo Lamberti, C. *J. Chem. Soc., Dalton Trans.* **2013**, *42*, 6564−71.
(45) Hecker, C. R.; Fanwick, P. E.; McMillin, D. R. *Inorg. Chem.* **1991**, *30*, 659−666.
(46) Osterman, T. E.; Abrahamsson, M.; Becker, H.-C.; Hammarstr €om, L.; Persson, P. *J. Phys. Chem. A* **2012**, *116*, 1041−50.
(47) Daniel, C. *Coord. Chem. Rev.* **2003**, *238*−*239*, 143−166.
(48) Sun, S.; Mosquera-Vazquez, S.; Daku, L. M. L. G. L.; Goodwin, H. A. V. E.; Hauser, A. *J. Am. Chem. Soc.* **2013**, *00*, 00.
(49) Tsai, C. N.; Tian, Y.-H.; Shi, X.; Lord, R. L.; Schlegel, H. B.; Chen, Y. J.; Endicott, J. F. *Inorg. Chem.* **2013**, *52*, 9774−90.
(50) (a) Alary, F.; Heully, J.; Bijjeire, L.; Vicendo, P. *Inorg. Chem.* **2007**, *46*, 3154−65. (b) Borg, O. A.; Godinho, S. S. M. C.; Lundqvist, M. J.; Lunell, S.; Persson, P. *J. Phys. Chem. A* **2008**, *112*, 4470−76.
(51) Chen, J.; Chi, Y.; Chen, K.; Cheng, Y.-M.; Chung, M.-W.; Yu, Y.-C.; Lee, G.-H.; Chou, P.-T.; Shu, C.-F. *Inorg. Chem.* **2010**, *49*, 823−32.
(52) GoØttle, A. J.; Dixon, I. M.; Alary, F.; Heully, J. L.; Boggio-Pasqua, M. *J. Am. Chem. Soc.* **2011**, *133*, 9172.
(53) Alary, F.; Boggio-Pasqua, M.; Heully, J.-L.; Marsden, C. J.; Vicendo, P. *Inorg. Chem.* **2008**, *47*, 5259−5266.
(54) Litke, S. V.; Mezentseva, T. V.; Lyalin, G. N.; Ershov, A. Y. *Opt. Spektrosk.* **2003**, *95*, 980−7.
(55) Chun-Ying, D.; Zhong-Lin, L.; Xiao-Zeng, Y.; Mak, T. C. W. *J. Coord. Chem.* **1999**, *46*, 301−312.
(56) Tondreau, M.; Milsmann, C.; Lobkovsky, E.; Chirik, P. J. *Inorg. Chem.* **2011**, *50*, 9888.
(57) Dixon, I. M.; Alary, F.; Heully, J.-L. *J. Chem. Soc., Dalton Trans.* **2010**, *39*, 10959−966.
(58) Durham, W.; Wilson, S. R.; Hodgson, D. J.; Meyer, T. J. *J. Am. Chem. Soc.* **1980**, *102*, 600−607.
(59) Johnson, E. S.; Sullivan, B. P.; Salmon, D. J.; Adeyemi, A.; Meyer, T. J. *Inorg.Chem.* **1978**, *17*, 2211.
(60) Durham, W.; Walsh, J. L.; Carter, C. L.; Meyer, T. J. *Inorg. Chem.* **1980**, *19*, 860−65.
(61) Camilo, M. R.; Martins, F. T.; Malta, V. R. S.; Ellena, J.; Carlos, R. M. *Acta Crystallogr., Sect. E: Struct. Rep. Online* **2013**, *E69*, m75m76.
(62) Rillema, D. P.; Jones, D. S.; Woods, C.; Levy, H. A. *Inorg. Chem.* **1992**, *31*, 2935−2938.

(63) Stoyanov, S. R.; Villegas, J. M.; Rillema, D. P. *Inorg. Chem.* **2002**, *41*, 2941−2945.
(64) Lever, A. B. P. *Inorganic Electronic Spectroscopy;* Elsevier Science: Amsterdam, 1984.
(65) Juris, A.; Balzani, V.; Barigelletti, F.; Campagna, S.; Belser, P.; Zelewsky, A. v. *Coord. Chem. Rev.* **1988**, *84*, 85−277.
(66) Odongo, N. S.; Heeg, M. J.; Chen, Y.-J.; Xie, P.; Endicott, J. F. *Inorg. Chem.* **2008**, *47*, 7493−7511.
(67) Foxon, S. P.; Alamiry, M. A. H.; Walker, M. G.; Meijer, A. J. H. M.; Sazanovich, I. V.; Weinstein, J. A.; Thomas, J. A. *J. Phys. Chem. A* **2009**, *113*, 12754−12762.
(68) Sun, Y.; El, O. M.; Hammitt, R.; Thummel, R. P.; Turro, C. *J. Phys. Chem.* **2010**, *114*, 14664−14670.
(69) Lutterman, D. A.; Lazinski-Melanson, L. A.; Asher, Y.; Johnston, D. H.; Gallucci, J. C.; Turro, C. *J. Photochem. Photobiol., A* **2011**, *217*, 2011.
(70) Lachish, U.; Infelta, P. P.; Grätzel, M. *Chem. Phys. Lett.* **1979**, *62*, 317.
(71) Bensasson, R.; Salet, C.; Balzani, V. *J. Am. Chem. Soc.* **1976**, *98*, 3722.
(72) Tarnovsky, A. N.; Gawelda, W.; Johnson, M.; Bressler, C.; Chergui, M. *J. Phys. Chem. B.* **2006**, *110*, 26497−26505.
(73) Sato, S.; Sekine, A.; Ohashi, Y.; Ishitani, O.; Blanco-Rodriguez, A. M.; Vlĉek, A., Jr.; Unno, T.; Koike, K. *Inorg. Chem.* **2007**, *46*, 3531−3540.
(74) (a) Gabrielsson, A.; Zalis, S.; Matousek, P.; Towrie, M.; Vlĉek, A., Jr. *Inorg. Chem.* **2004**, *43*, 7380−7388. (b) Gabrielsson, A.; Towrie, M.; Zalis, S.; Vlĉek, A. *Inorg. Chem.* **2008**, *47*, 4236−4242.
(75) Dodsworth, E. S.; Lever, A. B. P. *Chem. Phys. Lett.* **1986**, *124*, 152−8.
(76) Lever, A. B. P. *Inorg. Chem.* **1990**, *29*, 1271−1285.
(77) Sizova, O. V.; Baranovskii, V. I.; Ershov, A. Yu.; Sizov, V. V.; Shashko, A. D.; Nikol'skii, A. B. *Russ. J. Gen. Chem.* **2001**, *71*, 1194−1202.
(78) Rimmer, R. D.; Pierri, A. E.; Ford, P. C. *Coord. Chem. Rev.* **2012**, *256*, 1509.
(79) Ramírez, C. L.; Pegoraro, C. N.; Filevich, O.; Bruttomeso, A.; Etchenique, R.; Parise, A. R. *Inorg. Chem.* **2012**, *51*, 1261−68.
(80) Noodleman, L.; Lovell, T.; Han, W. G.; Liu, T.; Torres, R. A.; Himo, F. Chapter 2.39. In *Comprehensive Coordination Chemistry II;* Elsevier Science Publishers: Amsterdam, 2004; pp 491−510.
(81) Bickelhaupt, F. M.; Baerends, E. J. *Reviews in Computational Chemistry;* Lipkowitz, K. B., Boyd, D. R. E., Eds.; Wiley: New York, 2000; Vol. *15*, pp 1−86.
(82) McKinnon, S. D. J.; Patrick, B. O.; Lever, A. B. P.; Hicks, R. G. *J. Am. Chem. Soc.* **2011**, *133*, 13587−603.
(83) Lever, A. B. P.; Gorelsky, S. I. *Coord. Chem. Rev.* **2000**, *208*, 153−167.
(84) Gorelsky, S. I.; Lever, A. B. P.; Ebadi, M. *Coord. Chem. Rev.* **2002**, *230*, 97−105.
(85) Gorelsky, S. I.; Lever, A. B. P. *J. Organomet. Chem.* **2001**, *635*, 187−196.
(86) Li, J.; Xu, L.-C.; Chen, J.-C.; Zheng, K.-C.; Ji, L.-N. *J. Phys. Chem. A* **2006**, *110*, 8174−80.
(87) Remenyi, C.; Kaupp, M. *J. Am. Chem. Soc.* **2005**, *127*, 11399−11413.
(88) Al-Noaimi, M.; El-khateeb, M.; Haddad, S. F.; Sunjuk, M.; Crutchley, R. J. *Polyhedron* **2008**, *27*, 3239−46.
(89) Ess, D. H.; Gunnoe, T. B.; Cundari, T. R.; Goddard, W. A. I.; Periana, R. A. *Organometallics* **2010**, *29*, 6801−6815.
(90) Futera, Z.; Klenko, J.; Sponer, J. E.; Sponer, J.; Burda, J. V. *J. Comput. Chem.* **2009**, *30*, 1758−70.
(91) Scuppa, S.; Orian, L.; Donoli, A.; Santi, S.; Meneghetti, M. *J. Phys. Chem. A* **2011**, *115*, 8344−49.
(92) Bossert, J.; Daniel, C. *Coord. Chem. Rev.* **2008**, *252*, 2493−2503.
(93) Dallinger, R. F.; Woodruff, W. H. *J. Am. Chem. Soc.* **1979**, *101*, 4391−4393.
(94) McCusker, J. K. *Acc. Chem. Res.* **2011**, *36*, 876−887.
(95) Campagna, S.; Puntoriero, F.; Nastasi, F.; Bergamini, G.; Balzani, V. *Topics. Curr. Chem.* **2007**, *280*, 117.
(96) Abrahamsson, M.; JaØ ger, M.; Kumar, R. J.; OØsterman, T.; Persson, P.; Becker, H.-C.; Johansson, O.; HammarstroØm, L. *J. Am. Chem. Soc.* **2008**, *130*, 15533−42.
(97) Medlycott, E. A.; Hanan, G. S. *Coord. Chem. Rev.* **2006**, *250*, 1763−82.
(98) *Photophysics of Organometallics: 29 (Topics in Organometallic Chemistry);* Lees, A. J., Ed.; Springer: New York, 2010.
(99) (a) Guillon, T.; Boggio-Pasqua, M.; Alary, F.; Heully, J. L.; Lebon, E.; Sutra, P.; Igau, A. *Inorg. Chem.* **2010**, *49*, 8862−8872. (b) Piau, R. E.; Guillon, T.; Lebon, E.; Perrot, N.; Alary, F.; Boggio-Pasqua, M.; Heully, J.-L.; Juris, A.; Sutra, P.; Igau, A. *New J. Chem.* **2012**, *36*, 2484−2492.
(100) Glendening, E. D.; Landis, C. R.; Weinhold, F. *J. Comput. Chem.* **2013**, *34*, 1429−37.
(101) Daniel, C. *Coord. Chem. Rev.* **2002**, *230*, 65−78.
(102) Dattelbaum, D. M.; Martin, R. L.; Schoonover, J. R.; Meyer, T. J. *J. Phys. Chem. A* **2004**, *108*, 3518−3526.
(103) Watzky, M. A.; Macatangay, A. V.; Vancamp, R. A.; Mazzetto, S. E.; Song, X. Q.; Endicott, J. F.; Buranda, T. *J. Phys. Chem. A.* **1997**, *101*, 8441−8459.
(104) Vlĉek, A. *Coord. Chem. Rev.* **2000**, *200−202*, 933−978.
(105) Allard, M. M.; Odongo, O. S.; Lee, M. M.; Chen, Y.-J.; Endicott, J. F.; Schlegel, H. B. *Inorg. Chem.* **2010**, *49*, 6840−52.
(106) Chen, Y.-J.; Odongo, O. S.; McNamara, P. G.; Szacilowski, K. T.; Endicott, J. F. *Inorg. Chem.* **2008**, *47*, 10921.
(107) Connelly, N.; Geiger, W. *Chem. Rev.* **1996**, *96*, 877−910.
(108) (a) Rabek, J. F. *Experimental Methods in Photochemistry and Photophysics;* Wiley: New York, 1982. (b) Calvert, J. G.; Pitts, J. N. *Photochemistry;* John Wiley and Sons: New York, 1967.
(109) Hungerford, G.; Birch, D. J. S. *Meas. Sci. Technol.* **1996**, *7*, 121−135.
(110) Frisch, M. J.; et al. *Gaussian 09;* Gaussian, Inc.: Wallingford, CT, 2009.
(111) Lee, C.; Yang, W.; Parr, R. G. *Phys. Rev. B* **1988**, *37*, 785−789.
(112) Dunning, Jr. T. H.; Hay, P. J. *Modern Theoretical Chemistry;* H.F. Schaefer, I., Ed.; Plenum: New York, 1976; Vol. *3*, p 1.
(113) Hay, P. J.; Wadt, W. R. *J. Chem. Phys.* **1985**, *82*, 299−310.
(114) Hay, P. J.; Wadt, W. R. *J. Chem. Phys.* **1985**, *82*, 284−98.
(115) Hay, P. J.; Wadt, W. R. *J. Chem. Phys.* **1985**, *82*, 270−283.
(116) Van Gisbergen, S. J. A.; Baerends, E. J. *Comprehensive Coordination Chemistry II;* McCleverty, J. A., Meyer, T. J., Eds.; Pergamon: Oxford, 2003; pp 511−517.
(117) Grimme, S. *Rev. Comput. Chem.* **2004**, *20*, 153−218.
(118) Gorelsky, S. I. *SWIZARD;* CCRI, University of Ottawa: Ottawa, Canada, 2008. http://www.sg-chem.net/.
(119) Gorelsky, S. I. *AOMix-CDA Program*, CCRI, University of Ottawa: Ottawa, Canada, 2005. http://www.Sg-Chem.Net/.